Title
Improved Fuel Transport Selectivity in Polymer Electrolyte Membranes

Author
Clark, Kyle Tyler

Publication Date
2014

Peer reviewed|Thesis/dissertation

Improved Fuel Transport Selectivity in Polymer Electrolyte Membranes

By

Kyle Tyler Clark

A dissertation submitted in partial satisfaction of the

requirements for the degree of

Doctor of Philosophy

in

Engineering - Materials Science and Engineering

in the

Graduate Division

of the

University of California, Berkeley

Committee in charge:

Professor Thomas Devine, Co-chair
Dr. John Kerr, Co-chair
Professor Ting Xu
Professor Bryan McCloskey

Fall 2014

Abstract

Improved Fuel Transport Selectivity in Polymer Electrolyte Membranes

by

Kyle Tyler Clark

Doctor of Philosophy in Materials Science & Engineering

University of California, Berkeley

Professor Tom Devine, Co-chair

Dr. John Kerr, Co-chair

In polymer electrolyte membrane (PEM) fuel cells, fuel crossover through the membrane is a significant problem that contributes to reduction in cell efficiency and accelerated membrane degradation. The need for high water content in the membrane to produce acceptable conductivities leads to excessive fuel crossover while also limiting cell operating temperature to <100°C where platinum catalysts are easily contaminated by CO. This work focused on the study of transport functions in PEMs in an effort to reduce fuel crossover through the replacement of water with an alternative proton solvent.

The heterocycle imidazole was incorporated into Nafion® membranes as an alternative proton solvent because of its ability to form hydrogen bond networks similar to water, and its high proton conductivity (10^{-2} to 10^{-1} S/cm) at temperatures around 150°C. Imidazole must be covalently bonded to the membrane to prevent loss due to leeching by water, or sublimation at high temperatures. In this work, imidazole in the form of 4(5)-hydroxymethyl imidazole (ImOH) was imbibed into the perfluorosufonic acid membrane, Nafion®.

In this work, incorporation of ImOH into the membranes is shown improved the thermo-mechanical properties, as studied using dynamic mechanical analysis, while reducing water and methanol transport kinetics, as observed using dynamic vapor sorption and nuclear magnetic resonance. Study of the membrane using small angle x-ray scattering linked these results to changes in membrane morphology. Ex-situ study of methanol transport through the membrane was confirmed using in-situ electrochemical fuel crossover measurements on operational direct methanol fuel cells. The results showed that the use of ImOH as an immobilized proton solvent results in around a 50% reduction in methanol fuel crossover.

Contents

List of Figures

List of Tables

Chapter 1

Introduction

1.1 Background

Climate change and the ever increasing demand for energy is driving us towards an alternative energy economy based on intermittent power sources, such as, wind and solar. Due to the intermittent nature of these sources, there is a strong need to develop effective devices for energy storage. Hydrogen polymer electrolyte membrane fuel cells (PEMFCs) are considered to be a viable system for mobile applications because of the high theoretical energy density of hydrogen. However, challenges associated with the storage, transport, and distribution of hydrogen significantly decreases the advantages of energy density, and would require the construction of an expensive new infrastructure.

Direct methanol fuel cells (DMFCs) have a lower energy density than hydrogen PEMFCs and the performance is greatly degraded by fuel crossover. However, the use of a liquid fuel compatible with our liquid fuel infrastructure makes the DMFC an attractive option. In order for DMFCs to become a truly viable option, significant advancements in polymer electrolyte membrane (PEM) technology must be made.

The PEM is a key component in the fuel cell. The bulk membrane must act as a chemical and electrical separator, while being an efficient proton conductor. Crossover of fuel (eg. methanol) through the membrane causes a reduction in cell performance, while permeation of oxygen and its reactive forms (such as hydrogen peroxide) through the membrane results in membrane degradation and side reactions with the fuel. In the catalyst layer (CL), the polymer must allow access of fuel to the reaction sites, while facilitating rapid transfer of protons and electrons. Although the demands on these membranes seem high, perfluorinated sulfonic acid (PFSA) membranes, such as Nafion®, perform this role well enough for these devices to be built and operated.

This dissertation focuses on the study of transport functions in the bulk polymer membrane in order to improve membrane fuel transport selectivity.

1.2 Description of a Fuel Cell

A fuel cell is an electrochemical device that combines a fuel and oxygen to generate electricity. Figure 1.1 shows a schematic of a typical fuel cell. The anode and cathode are separated by a polymer electrolyte membrane (PEM). Fuel (e.g. methanol) is supplied to the anode where it is oxidized in the anode catalyst layer (CL), producing protons and electrons. The protons move through the PEM to the cathode, while the electrons travel through an external circuit before reaching the cathode. At the cathode, protons, electrons, and oxygen electrochemically react in the cathode CL producing water, and heat due to the inefficiency of the electrode reactions.

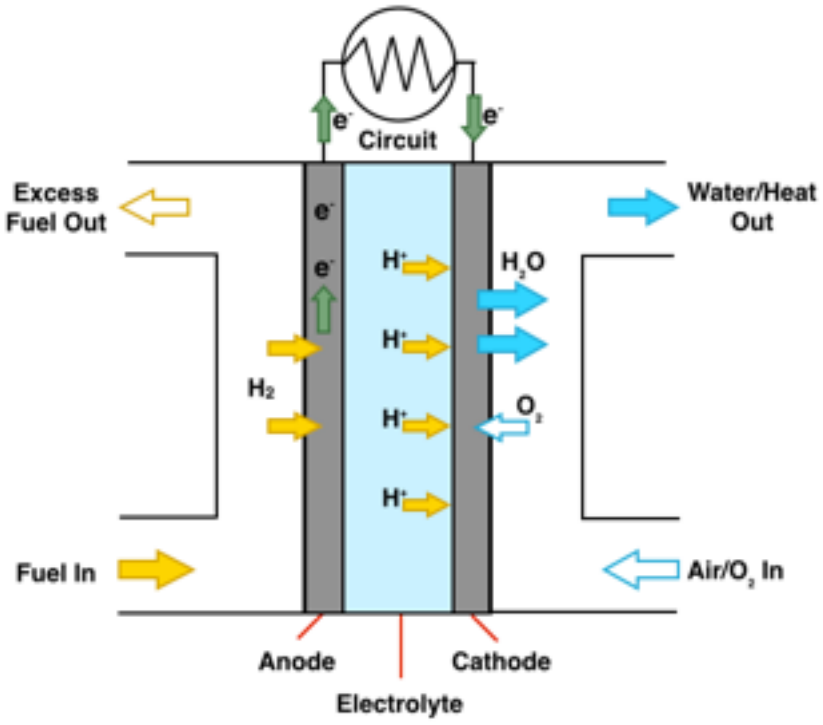

Figure 1.1: Schematic of a typical PEM fuel cell.

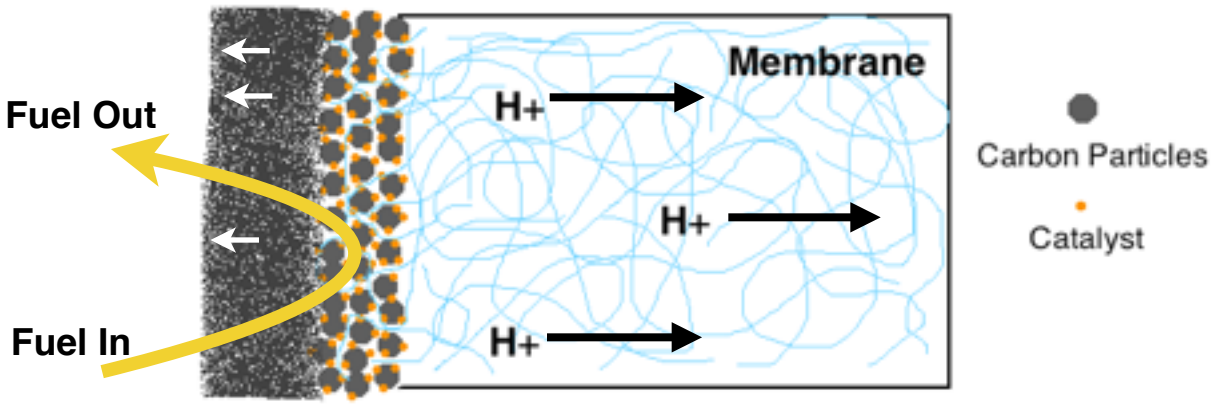

Figure 1.2: Schematic of the diffusion layer (DL), catalyst layer (CL), and membrane showing movement of protons, electrons, reactant, and product through the membrane-electrode interface.

1.2.1 Electrodes

In a fuel cell, the electrochemical reactions occur at the electrodes which have three main components: the electrocatalysts, the catalyst layer (CL), and the gas diffusion layer (GDL). The most widely used electrocatalysts are platinum based. The catalyst is typically supported on carbon black or carbon nanotubes, which have large surface areas and good electronic conductivity. The carbon supported catalyst is dispersed in the CL.

The CL is a thin, porous layer in which the electrochemical reactions occur. The CL is composed of the carbon supported catalyst powder and a proton conducting ionomer (eg. Nafion®). The structure of the CL must allow for proton and electron transport to and from the catalytic sites, and allow for reactant transport and product removal through the layer.

The GDL is a carbon fiber based material such as carbon paper or carbon cloth. It serves as support for the CL. The porosity of the GDL allows for the free flow of reactants and products to the CL, and the high conductivity of the carbon material provides good electronic contact with the external circuit.

When combined, these components make up the gas diffusion electrode (GDE). A schematic of the GDE is shown in Figure 1.2.

1.2.2 Polymer Electrolytes

At the center of the fuel cell is the polymer electrolyte membrane. The PEM serves two functions in the cell. The first is as an electrolyte through which protons are transported, and second as an electrical and chemical separator between the anode and cathode.

Commonly used PEMs are perfluorosulfonic acid (PFSA) membranes such as Nafion®. Nafion® is a commercially available PFSA membrane developed by DuPont in the late 1960s, and is still used as the baseline membrane for development of ion-conducting systems. Nafion® consists of a hydrophobic polytetrafluoroethylene (PTFE) backbone, providing mechanical stability, and sulfonic acid (SO_3^-) terminated side chains that phase separate from the PTFE backbone forming ionic-domains within the PTFE matrix (Molecular structure of Nafion® is shown in Figure 1.3). Exposure to water hydrates the ionic groups causing them to swell and become interconnected forming ion (H^+) conductive pathways (Figure 1.4). This hydrated, phase-separated structure is necessary for fuel cell performance[1-5].

The proton conductivity of the PFSA is highly dependent on the membrane's water content, with the highest conductivity occurring when water is in large excess over the sulfonic acid groups, $\lambda > 16$, where λ is the number of water molecules per sulfonic acid group[2]. It is the water-rich ionic pathways through the backbone structure that allows for fast proton transport via the structural diffusion of water (Grotthuss mechanism)[6-12]. Thermal, mechanical, and chemical stability of the membrane is a result of the PFSA backbone structure. The morphology created by the backbone

network also inhibits the transport of fuel and water through the membrane providing some selectivity.

Proton conductivity of the membrane is also related to the equivalent weight (EW) of the polymer. The EW is given as the weight of the polymer per available acid group, with Nafion® having an EW of ~1100 g/mol. Attempts to improve membrane conductivity by reducing the EW of the PFSA have been done, yielding a variety of short-side-chain polymers with EW as low as 550 g/mol. While these low equivalent weight membranes do show improved conductivity due to the increased sulfonic acid density, they suffer from reduced mechanical properties and swell significantly in water to the point of being nearly soluble in water[13].

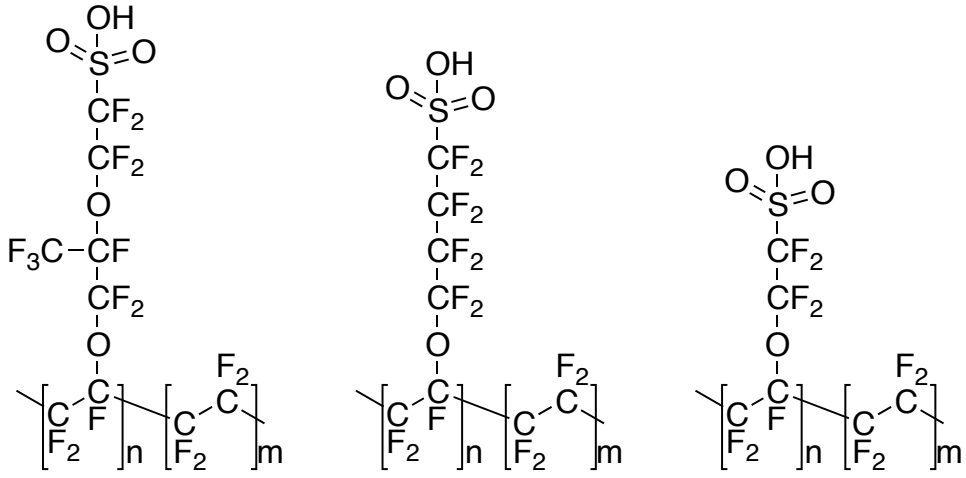

Figure 1.3: Molecular structures of PFSA with varying equivalent weights. EWs decrease in weight from left to right: Nafion® 1100EW (left), 3M 660-825EW (center), and Aquivion 600-900EW (right).

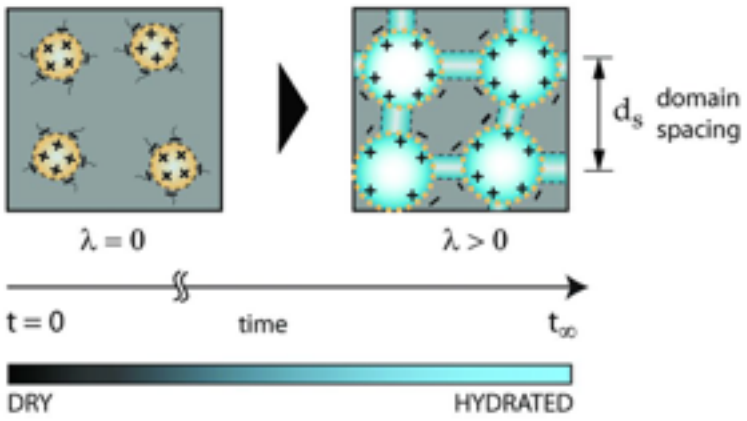

Figure 1.4: Swelling of hydrophilic nano-domains with increasing water content[1].

1.2.3 Membrane Electrode Assemblies

When the anode and cathode GDEs are attached to the PEM, they form the membrane electrode assembly (MEA). The MEA is the core component of the fuel cell as it provides sites for the electrochemical reactions and facilitates proton and electron transport within the cell. The GDEs are typically attached to the membrane by hot pressing. During this process, the GDEs are placed on either side of the membrane, forming a layered structure: anode GDL, anode CL, membrane, cathode CL, cathode GDL. The assembly is placed under pressure and heated to a temperature high enough to allow for mobility of the polymer chains within the membrane to make a good connection between the membrane and the CLs.

Good contact between the CLs and the PEM is important, as the CL/PEM interface can lead to high contact resistances, decreasing fuel cell performance. The CL is a *three phase* reaction site involving fuel/reactant, carbon supported catalyst, and ionomer. Hot pressing allows for the PEM to make good connection with the ionomer in the CL providing a continuous pathway for protons to move between the CL and the membrane.

1.3 Direct Methanol Fuel Cells

1.3.1 Methanol as a Fuel

Methanol has a few distinct advantages over hydrogen for use as a fuel, namely its high theoretical energy density of 6100 Wh/kg, and it is a liquid with a boiling point of 67.4°C, so no special cooling treatment is required making it reasonably compatible with existing liquid fuel infrastructure[14, 15].

Methanol is supplied to the anode where it is oxidized on the surface of a Pt/Ru catalyst releasing 6 protons and 6 electrons (1). At the cathode, oxygen is reduced at a Pt catalyst producing water (2). The overall reaction (3) can produce a theoretical open circuit voltage of 1.21V at room temperature with a theoretical reaction efficiency of almost 97%[14, 16, 17]. However, in practice, DMFCs perform well below theoretical efficiency due to high fuel crossover through the membrane, and poor electrochemical kinetics.

$$CH_3OH + H_2O \xrightarrow{Pt/Ru} CO_2 + 6H^+ + 6e^- \quad (1)$$

$$\frac{3}{2}O_2 + 6H^+ + 6e^- \xrightarrow{Pt} 3H_2O \quad (2)$$

$$CH_3OH + \frac{3}{2}O_2 \rightarrow CO_2 + 2H_2O \quad (3)$$

1.3.2 Fuel Cell Performance

Fuel cell performance is commonly characterized using a polarization curve to understand the relation between cell voltage and current density. A typical polarization curve obtained during a controlled current experiment for a DMFC is shown in Figure 1.5.

In the ideal cell, voltage is independent of current drawn. However, in practice there are several losses associated with fuel cell operation that reduce the cell voltage as current is increased. The first loss is a result of mixed potential at the electrodes (1). At open circuit voltage, unintended reactions occur and decrease electrode potential. The dominant cause of mixed potential is the high methanol crossover through the membrane from anode to cathode. At low current densities, the cell suffers from activation polarization (2). This is a result of poor reaction kinetics at the electrodes, predominately the slow oxidation of methanol at the anode[16, 18], although the oxygen reduction reaction at the cathode is also notoriously slow. At intermediate current densities, loss is a result of ohmic polarization (3). Here, losses are caused by the ohmic resistance of the cell, which is dominated by the resistance of the polymer electrolyte, and follows a $V = IR$ behavior. The ohmic resistance of the cell is easily determined using impedance spectroscopy at the intermediate current densities. Finally, at high current densities, concentration polarization occurs (4) due to mass transport limitations in the diffusion layers of the electrodes[16, 18-20].

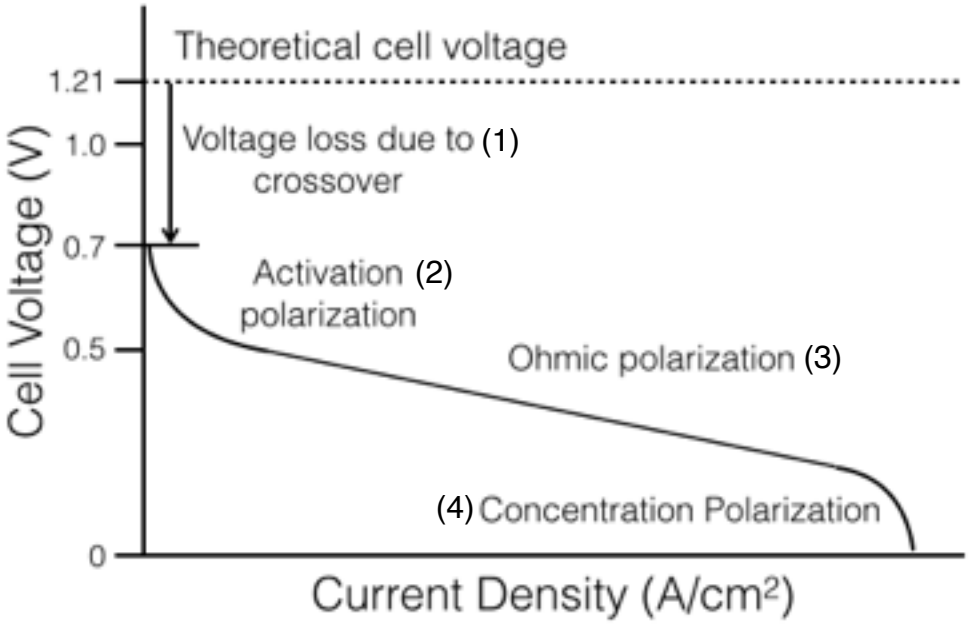

Figure 1.5: Typical polarization curve for a direct methanol fuel cell.

1.3.3 Methanol Crossover

As mentioned in the previous section, methanol crossover through the membrane results in a significant loss in cell open circuit voltage. The high rate of methanol crossover causes several major issues including parasitic reactions at both electrodes as well as accelerated membrane degradation[18 20, 23].

Methanol crossover is largely related to the membrane's dependence on the presence of water for conductivity. PFSA membranes need to be well hydrated in order for effective proton conduction to occur[7, 9, 12]. The water channels through which proton conduction occurs, also provide a pathway for methanol to move across the membrane with the water.

There are two modes of methanol transport across the membrane: diffusion and electro-osmotic drag by protons (Figure 1.6). At open circuit conditions, the methanol concentration gradient across the membrane drives the diffusion of methanol through these hydrated channels from anode to cathode[4, 21]. During fuel cell operation, the movement of protons through the membrane results in the transport of water across the membrane via electro-osmotic drag. The effects of electro-osmotic drag on water transport through Nafion® has been well studied, and has shown that each proton that moves across the membrane is accompanied by 2.5 water molecules[4, 16, 21, 22]. This means that for each methanol molecule oxidized at the anode, 15 water molecules are dragged across the membrane to the cathode, carrying methanol with them.

There has been recent work into the development of more active methanol oxidation catalysts[16, 24, 25]. In theory, this would reduce the methanol concentration at the membrane surface by completely oxidizing the methanol in the anode catalyst layer, leaving no methanol to cross through the membrane. Alternatively, the development of a more selective, less permeable, membrane is desirable in order to reduce the rate of methanol crossover.

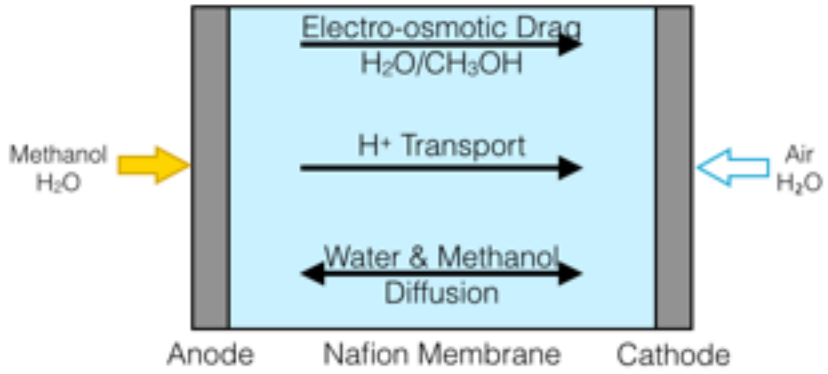

Figure 1.6: Schematic of modes of water and methanol transport across the membrane.

1.4 Previous Work on Polymer Electrolyte Membranes

1.4.1 Water Replacement

Current state-of-the-art PFSA membranes, like Nafion®, are highly dependent on water to achieve the level of proton conductivity necessary for operation in a fuel cell. The problems associated with this reliance on water, such as water management within the cell and electro-osmotic flow, make it appealing to develop a membrane that conducts protons in the absence of water. A water free membrane would not allow for electro-osmotic flow, thus removing a primary mode of methanol transport across the membrane.

Previous work from the Kerr Group at Lawrence Berkeley National Lab has shown that the addition of imidazole to a PFSA membrane, developed by 3M, results in reasonable conductivities (Figure 1.7)[26]. This is particularly true when imidazole is used in excess over the sulfonic acid groups ($\lambda = 9$), a condition which is the same for water in a PFSA, where conductivities are greatest for high water content ($\lambda > 16$)[27, 28]. Imidazole is capable of acting as the proton solvating molecule, and achieves high conductivities, because the two nitrogens act equally as proton donors and acceptors (Figure 1.8), and imidazole forms a hydrogen bonded network similar to that of water[7, 9]. Proton mobility through the imidazole network is further promoted by the phase separated morphology of the PFSA membrane, which serves to align the molecules allowing for proton transport over large distances[7, 29].

The presence of imidazole in the membrane has also been shown to reduce water up-take. This effect has been attributed to the fact that water and imidazole have similar pKa and pKb values, which leaves little thermodynamic drive for the imidazole to be replaced by water. However, over time, the imidazole is gradually leeched out of the membrane or sublimes out at high temperatures, which makes it necessary to tether the imidazole to the polymer structure if the observed effects are to be maintained for any significant amount of time[26-28].

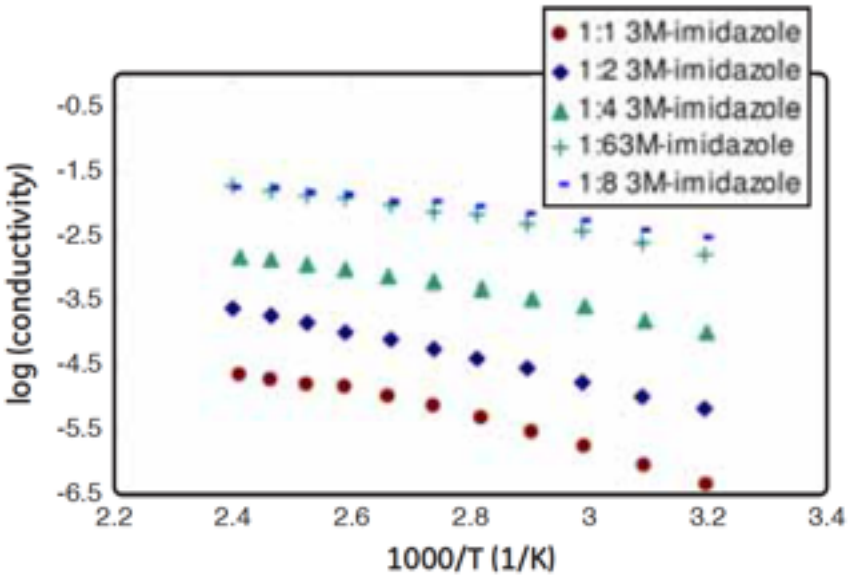

Figure 1.7: Proton conductivity of 3M PFSA-imidazole membranes with various acid to imidazole ratios under dry conditions[26].

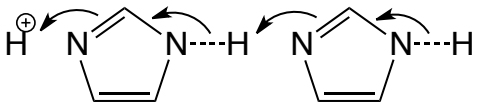

Figure 1.8: Proton transport between imidazole molecules. Both nitrogens are capable of acting as both a proton donor and acceptor.

1.4.2 Immobilization of Imidazole

In order for imidazole to be used successfully as a water replacement in a PEM, it must be covalently bonded to the polymer structure to prevent loss from leeching or sublimation. Imidazole contains several carbon sites through which it can be attached to a variety of oligomer and polymer systems. Examples of some immobilized imidazole structures that have been studied are shown in Figure 1.9.

While it has been shown that reasonable conductivities are achieved when imidazole is added into the PFSA structure, immobilization of imidazole generally leads to a reduction in proton conductivity. However, many insights have been made into what kinds of attachment structures are favorable. For instance, the best conductivities are observed when the imidazole is attached to the polymer backbone via a short, flexible linker. Long attachments result in dilution of the imidazole groups, decreasing proton conductivity[7, 30].

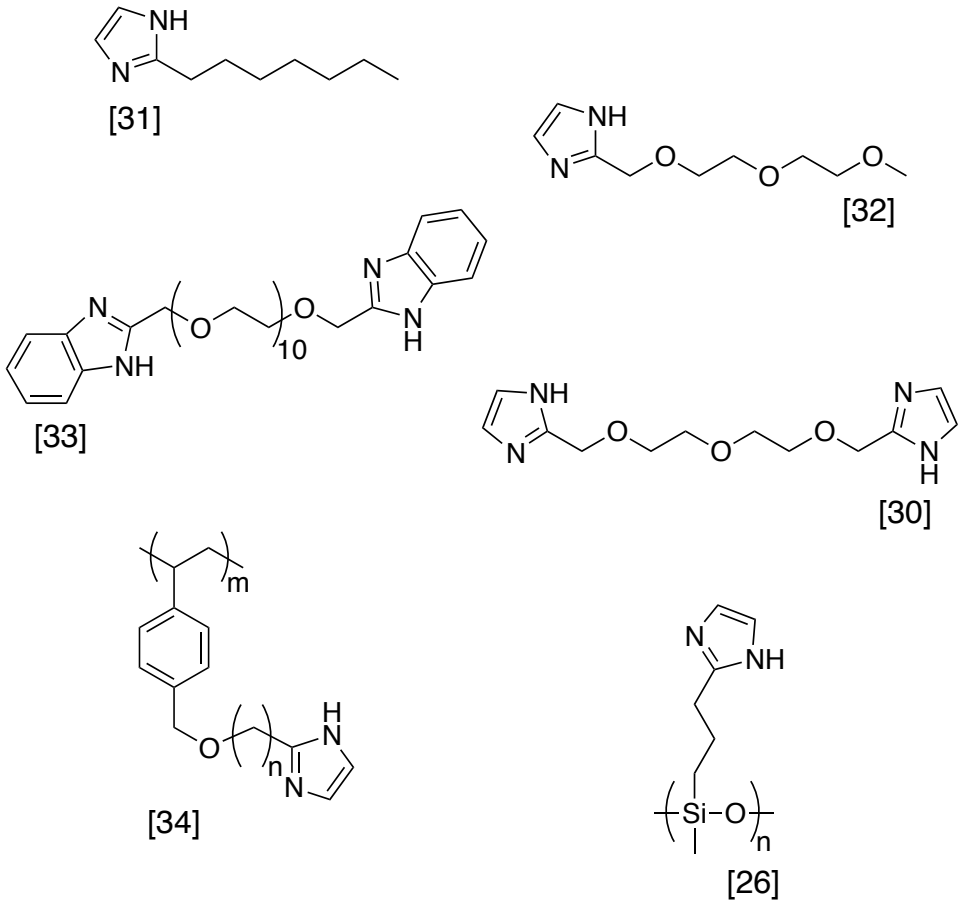

Figure 1.9: Examples of immobilized imidazole based systems used in polymer electrolyte membranes

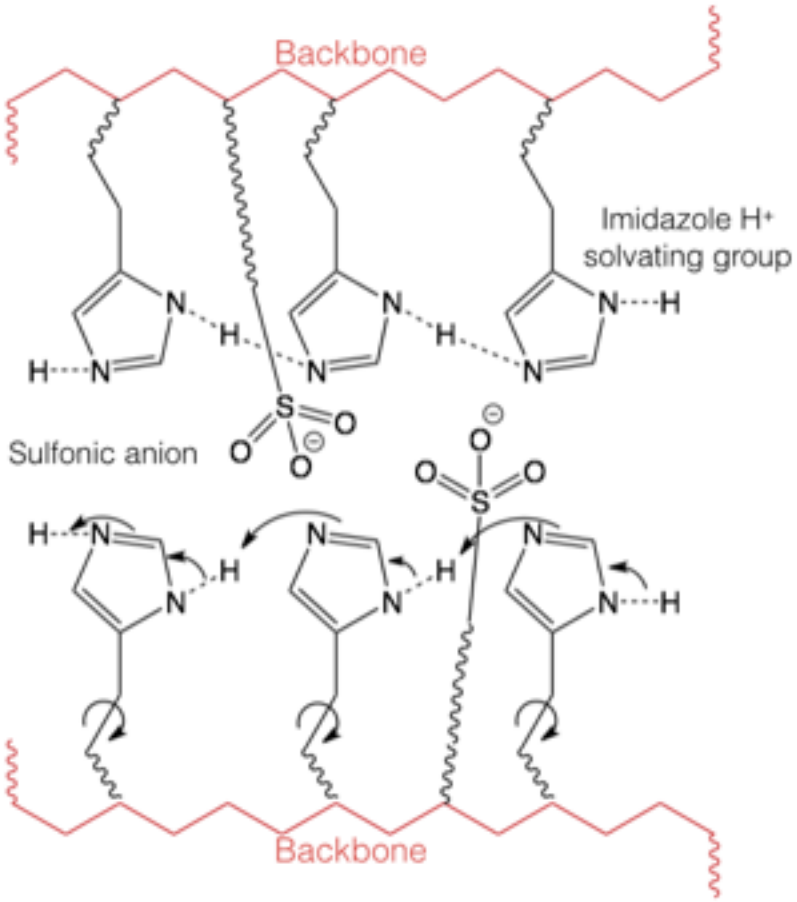

Figure 1.10: Schematic of proton transport through a membrane with acid and immobilized imidazole groups.

Figure 1.10 shows a schematic of a polymer structure in which imidazole is covalently attached to a flexible side chain. Attachment of the imidazole in this fashion would prevent it from washing out of the membrane while allowing for the motion necessary to facilitate proton conduction. The flexibility of the side chains allows for a certain amount of segmental motion to occur, carrying the proton through small portions of the membrane. Electronic rearrangement of the solvent molecule will facilitate proton transfer between molecules as shown by the arrows in Figure 1.10. The flexibility of the covalent attachment will allow for rotation of the imidazole group, allowing for protons to quickly hop between imidazoles[7].

The rotational motion of the imidazole groups is the preferred mode of proton transport because of the smaller mass associated with molecular rotation as compared with segmental motion. In order to best facilitate this mechanism, a bit of morphological control of the membrane is necessary. Selection of backbone type and side chain length can be used to promote molecular alignment of the imidazoles to promote proton mobility through the membrane[29].

While there have been many studies on the conductivity of polymer electrolyte systems containing imidazole and immobilized imidazole, studies on the selectivity of these membranes are limited, and are generally focused on the study of water up-take and behavior in hydrogen PEMFCs[7, 35].

In the interest of progressing the understanding of immobilized imidazole polymer electrolytes, we decided to study the effects of imidazole, immobilized in a PFSA structure, on membranes operating in DMFCs. In particular we are interested in how the incorporation of the imidazole effects the selective properties of the membrane in an effort to reduce the high methanol crossover that severely limits DMFC performance.

Overall, we aim to answer the following questions: How does attachment of imidazole to the PFSA structure affect membrane properties, such as, thermal stability, mechanical strength, solvent sorption, and morphology? Is an imidazole based PEM compatible with existing Pt based DMFC catalysts? Can these immobilized imidazole PFSA membranes perform in a DMFC? What effect does imidazole have on membrane selectivity to methanol transport? The answers to these questions will contribute to the design and development of future polymer electrolyte structures with immobilized proton solvents.

This work aims to characterize immobilized imidazole PFSA membranes and investigate their selectivity and performance in DMFCs. The results and experimental details of this study are presented in the following manner: Chapter 2 looks at the modification of Nafion® with imidazole, and discusses the effects on the thermal and mechanical properties of the membrane; Chapter 3 covers the effects imidazole modification has on the water up-take, conductivity, and membrane morphology; Chapter 4 discusses the behavior and performance of the membranes in a DMFC, as well as the effects on membrane selectivity to methanol transport; Chapter 5 looks at how compatibility of the imidazole membrane with current Pt-based DMFC catalysts can be improved; Chapter 6 outlines the experimental methods and procedures used while conducting this work.

Chapter 2

Modification, Thermal and Mechanical Properties of Nafion® 212 : 4(5)-hydroxymethyl Imidazole Membranes

2.1 Introduction

The main purpose of this work is to develop a polymer electrolyte membrane (PEM) with improved selectivity to fuel transport through the membrane. The primary pathway for methanol transport through the PEM is the water filled network of hydrophilic channels within the membrane via diffusion and electroosmotic drag[21, 22]. The membrane could be made more resistant to methanol transport by removing the water from the membrane. However, it is the water that provides a pathway for protons to move through the PEM structure. Therefore, it is desirable to replace water with a molecule that will prevent the movement of methanol through the membrane, while maintaining proton transport properties.

The use of imidazole in perfluorosulfonic acid (PFSA) type membranes has been shown to replace water as the proton conducting solvent within the membrane structure, as discussed in Section 1.4. However, the use of free imidazole has limited application due to the gradual loss of imidazole from leeching and sublimation[7, 36]. In order to prevent imidazole from washing out of the membrane, it is necessary to attach the imidazole to the membrane structure via a flexible covalent bond. In this chapter, imidazole is attached to the Nafion® structure by the formation of an ester between the sulfonic acid group of the Nafion® side chain and the hydroxyl group of 4(5)-hydroxymethyl imidazole (ImOH). The effects of ImOH modification on the thermal and mechanical properties of the membrane are investigated.

2.2 Discussion

2.2.1 Modification of Nafion® 212

4(5)-hydroxymethyl imidazole (ImOH) was added to as-received Nafion® 212 (N212) membranes as described in section 6.2.1. Proton and fluorine NMR studies, performed by graduate student Matt Dodd, showed that the nature of the bond between the ImOH and the sulfonic acid groups depends on the concentration of the ImOH in the membrane[37]. The structures, as determined by NMR, of the membranes are shown in Figure 2.1. The structure of N212 is shown in Figure 2.1a. The addition of ImOH to N212 in the 2:1 ratio results in two different bonds between the ImOH and the SO_3 groups, as shown in Figure 2.1b. Half of the SO_3^- groups form an ester with the hydroxy group of the ImOH. The remaining half of the SO_3 groups form a salt with the imidazole ring. Increasing the concentration of ImOH to the 1:1 ratio results in the formation of a salt with all SO_3^- groups, as shown in Figure 2.1c.

The difference in bonding between the two different ImOH ratios is due to the environment within the membrane. The nature of the SO_3^- groups in Nafion® make the membrane a superacid. Ester bond formation between the acid and the ImOH is favored in these acidic conditions. In the N212:ImOH 2:1 membrane, membrane acidity is high enough to favor stable ester bond formation. When the amount of ImOH is increased, as in the case for the N212:ImOH 1:1 membranes, the acidity of the membrane decreases to the point where ester bond formation is no longer favored, and a salt is formed between the membrane and the ImOH.

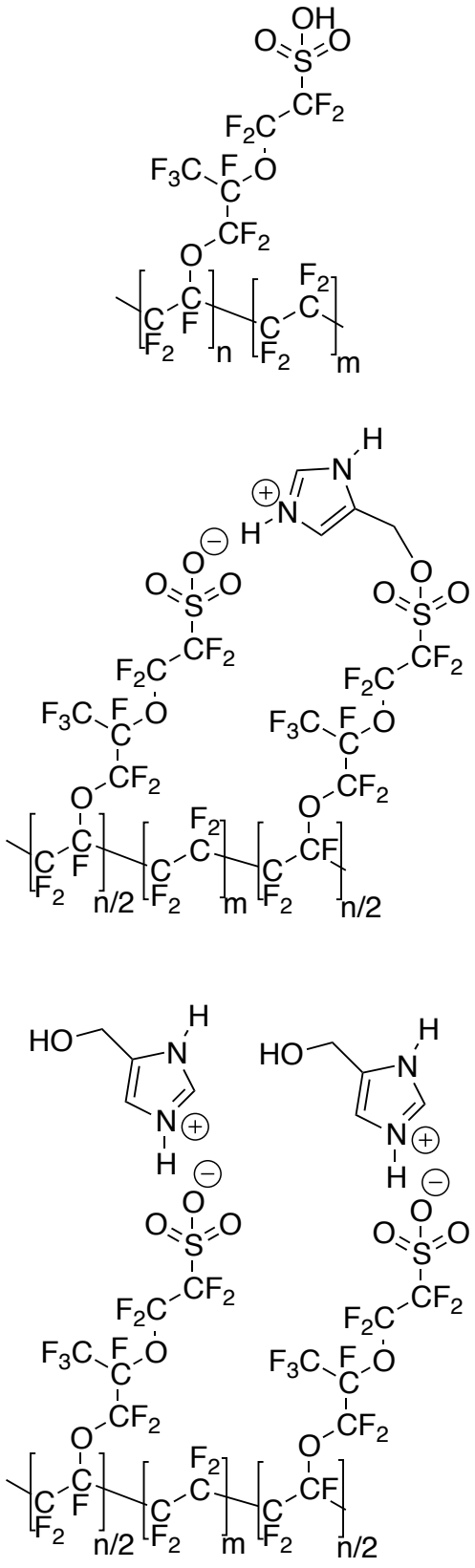

Figure 2.1: Polymer structure of N212 (a), N212:ImOH 2:1 (b), and N212:ImOH1:1(c).

2.2.2 Thermal Properties

Thermal stability of the ImOH modified Nafion® was measured with thermogravimetric analysis (TGA) between 50°C and 575°C under nitrogen atmosphere. The mass loss curve for Nafion® 212 is shown in Figure 2.2a. Three loss stages are observed, and are consistent with TGA results from the literature[38-40]. The initial mass loss below 250°C is due to residual water within the membrane absorbed from the air. Above 250°C the three loss stages observed in N212 are clearly seen in the first derivative of the TGA (Figure 2.2a). The onset temperature of the first loss stage occurs around 315°C and is attributed to a desulfonation process, while the second loss stage (390°C) is related to the degradation of the side chains, and the third loss (440°C) to decomposition of the PTFE backbone[38].

Figures 2.2b and 2.2c show the mass loss curves for N212:ImOH 2:1 and N212:ImOH 1:1 respectively. In Table 2.1, thermal behavior data for the Nafion® membranes is presented. It can be seen that the addition of ImOH to Nafion® changes the thermal properties of the membrane. Looking at the first derivative of the loss curves we see that the ImOH modified membranes exhibit only two distinct loss stages. The onset temperatures for the first and second stages of N212:ImOH 2:1 are 330°C and 409°C respectively, while for N212:ImOH 1:1 the temperatures are 355°C and 405°C respectively.

From observing the first loss stage, it is seen that increasing ImOH content corresponds to an increase in onset temperature. The formation of sulfonic esters and the ionic pairs $-SO_3^-$ $-ImOH^+$ appears to stabilize the C-S bonds delaying desulfonation until higher temperatures are reached.

The ImOH modified N212 membranes no longer exhibit three loss stages. Where the N212 had its second and third stages, the N212:ImOH 2:1 and 1:1 membranes now have a single loss stage at an intermediate temperature (409°C and 405°C respectively). Despite the final loss stage being about 40°C earlier than that of N212, the modified membranes do not complete thermal degradation until above 450°C, similar to N212. The addition of ImOH also resulted in increased residue weight stable to 575°C.

Below 250°C, all membranes showed a gradual mass loss due to water. This loss is greatest for the unmodified N212 membrane at about 4.1 wt%, while the water weight loss decreases with increasing ImOH content, with N212:ImOH 2:1 containing about 2.2 wt% water, and N212:ImOH 1:1 containing only 1.4 wt% water. It is already apparent from TGA measurements that the presence of ImOH in the membrane reduces the membrane water content, this will be discussed further in Section 3.2.1.

Table 2.1. Thermal behavior data as determined by TGA for Nafion® membranes in the temperature range of 50-575°C under nitrogen atmosphere. Mass loss (m), onset (T_O) and inflection point (T_{ip}) decomposition temperatures, and residue content are shown.

Sample	Stage	m (%)	T_O (°C)	T_{ip} (°C)	Residue at 575°C
N212	Water Loss	4.1			
	Loss 1	11.1	316	350	
	Loss 2	12.9	393	408	
	Loss 3	71.9	443	454	0%
N212:ImOH 2:1	Water Loss	2.2			
	Loss 1	15.7	329	353	
	Loss 2	77.8	409	433	4.3%
N212:ImOH 1:1	Water Loss	1.4			
	Loss 1	16.6	356	368	
	Loss 2	66.2	405	425	15.8%

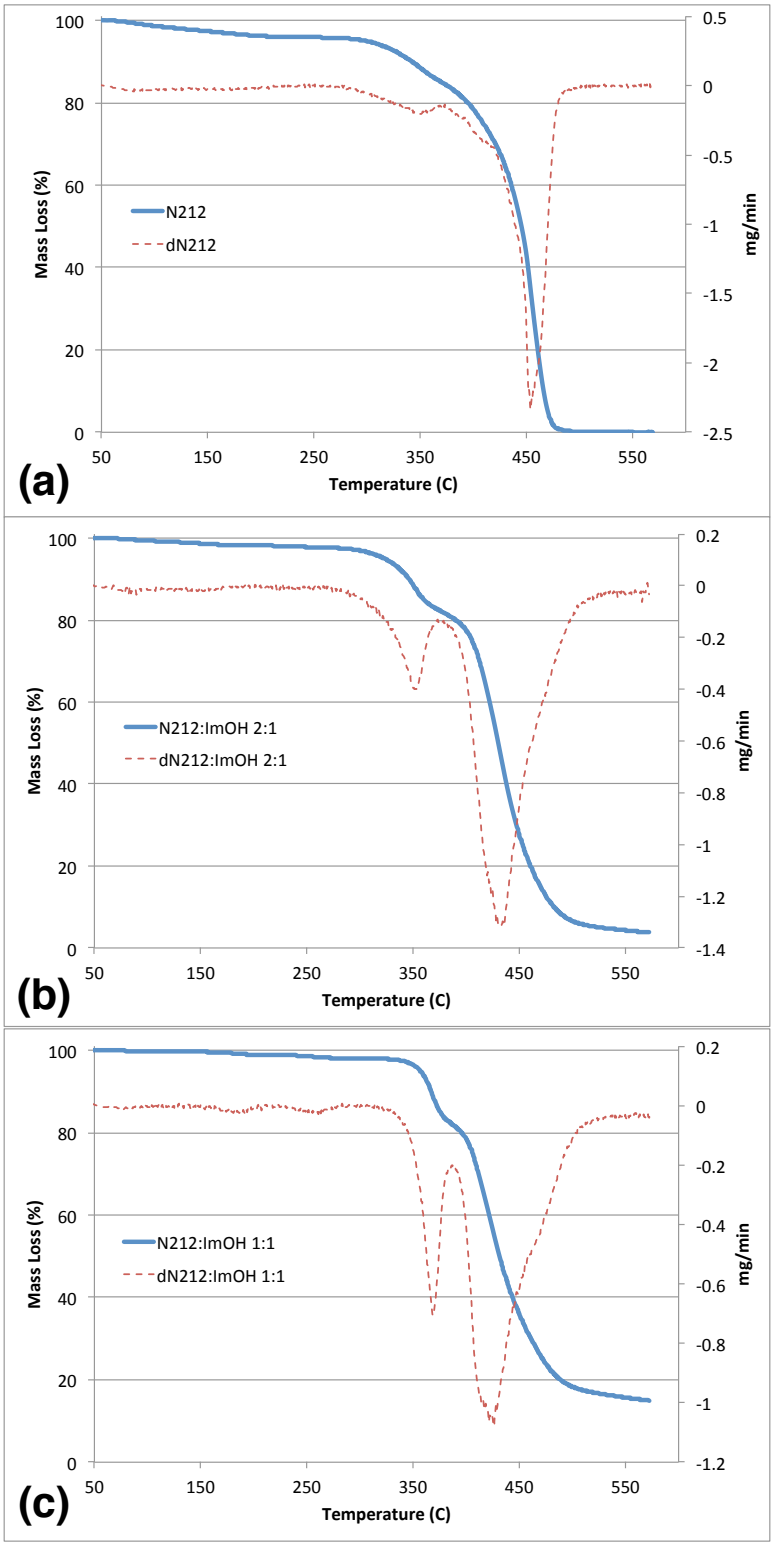

Figure 2.2: TGA mass loss curves (—) and dTGA (----) for N212 (a), N212:ImOH 2:1 (b), and N212:ImOH 1:1 (c) over the temperature range 50-575°C at 20°C/min under nitrogen atmosphere.

Thermal transitions were measured using differential scanning calorimetry (DSC) over the temperature range of -100°C to 200°C at a heating rate of 10°C/min under nitrogen atmosphere.The DSC traces of the second heating of Nafion® 212 (trace A), N212:ImOH 2:1 (trace B), and N212:ImOH 1:1 (trace C), in the same heat scale shifted along the ordinate, are shown in Figure 2.3. Trace A exhibits three thermal events. The first is an exothermic peak near -50°C (T_1) suggesting a crystalizing event, followed by two, more subtle, thermal events at about 0°C (T_2) and 100°C (T_3).

Looking at Trace C, we see that the thermal behavior of N212:ImOH 1:1 is similar to that of unmodified N212 with three thermal events observed at -50°C (T_1), 0°C (T_2), and 100°C (T_3). However, there is an additional transition near 150°C (T_4).

From Trace B, we see that there is a distinct difference in thermal behavior between the N212:ImOH 2:1 and 1:1. The T_1 transition in Trace B is an endothermic peak at about -50°C, suggesting a melting event where the other two membranes show a crystalizing event. A T_2 transition is also observed around 0°C, but as an exothermic step as compared to the endothermic steps of Trace A and C. The T_3 and T_4 transitions appear in a similar manner as those of Trace C.

The presence of the T_4 transition in Traces B and C, but not in Trace A, suggest that this is a thermal event related to the ImOH in the Nafion® structure, while the three shared events are likely thermal transitions related to the Nafion® structure. However, the more interesting event is the low temperature T_1 transition, where the N212:ImOH 2:1 membrane exhibits very different behavior from the other two. The difference in behavior of the T_1 transition in the N212:ImOH 2:1 as compared with the N212:ImOH 1:1 and unmodified Nafion® membranes suggests that this change in thermal behavior is not simply due to the presence of ImOH, but is also influenced by the way in which the ImOH interacts with the Nafion® membrane. This would be consistent with NMR observations discussed in Section 2.2.1, where a difference in bonding is seen between the 2:1 and 1:1 modifications (Figure 2.1).

In the N212:ImOH 1:1 membrane, NMR showed the formation of ionic bonds between the nitrogen of the imidazole ring and the sulfonic acid groups of Nafion®, forming a salt. Because of the similarities in pKa of imidazole and water, it is plausible that the interactions of the sulfonic acid groups with the water of the unmodified N212 or the imidazole of the N212:ImOH 1:1 result in similar thermal behavior at the T_1 transition.

For the N212:ImOH 2:1 membrane, NMR showed the presence of ester bonds between the sulfonic acid groups and the alcohol of ImOH. Ester bonds are structurally flexible, and the presence of these flexible bonds in place of the ionically bonded ImOH may be the cause of the change observed in the T_1 transition behavior.

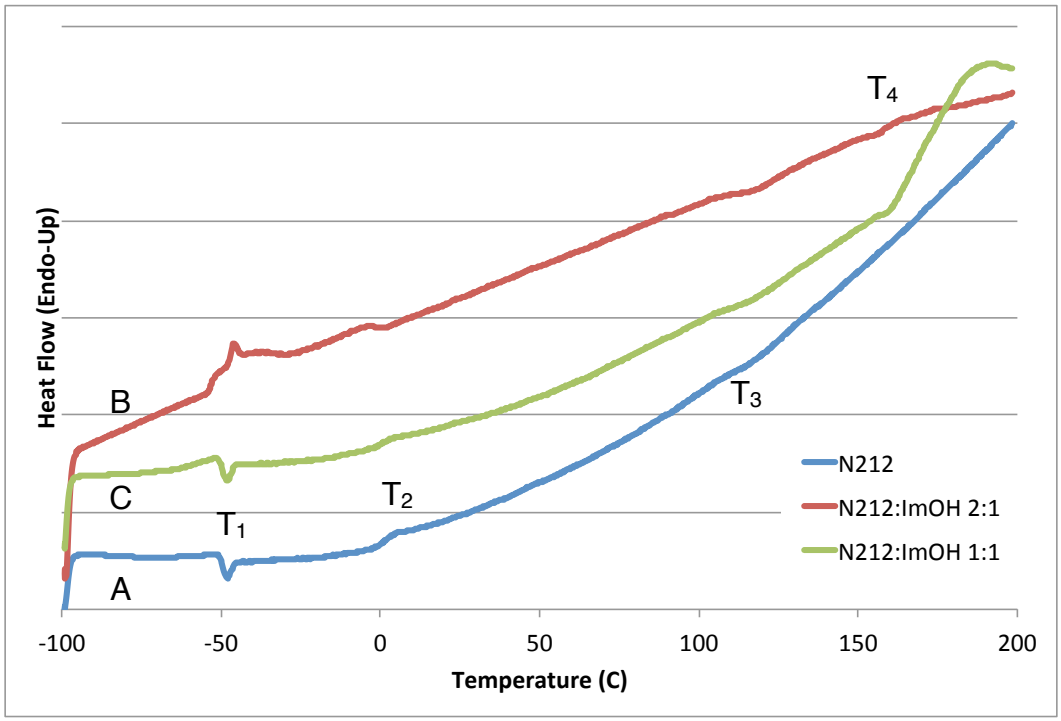

Figure 2.3: DSC traces of the second heating of N212 (trace A), N212:ImOH 2:1 (trace B), and N212:ImOH 2:1 (trace C), on the same heat scale and shifted along the ordinate, in the temperature range of -100°C to 200°C with heating rate 10°C/min.

2.2.3. Mechanical Properties

Mechanical measurements over the temperature range of -150°C to 200°C were carried out using dynamic mechanical analysis (DMA), as described in Section 6.1.4, to determine the effects of modification of N212 with ImOH on the mechanical stability of the membranes. Figure 2.4 compares DMA data of N212 (a), N212:ImOH 2:1 (b), and N212:ImOH 1:1 (c) for 0.1, 1.0, and 10 Hz as storage modulus (elastic response) and loss modulus (viscous behavior) on the left axis, and loss tangent on the right axis, vs temperature.

Figure 2.4A shows DMA data for N212, where it can be seen that the storage modulus (E') decreases three orders of magnitude, from $3.6x10^9$ Pa to $1.7x10^6$ Pa, over the temperature range shown. Decreases in the E' are related to various relaxations within the polymer structure, and are more easily seen as peaks in the loss modulus (E") or loss tangent (tan(δ)). Looking at Figure 2.4a, we see that at all frequencies, N212 exhibits a distinct α-relaxation near 100°C, as indicated by the prominent peak in tan(δ). A step is observed in the 0.1 Hz tan(δ) data just above 0°C representing a β-relaxation. All frequencies also show a γ-relaxation near -60°C. The α-, β-, and γ-relaxations appear at temperatures that correspond to the T_3, T_2, and T_1 DSC transitions respectively (Figure 2.3).

The relaxation temperature can be determined in two ways. The more commonly referenced values are taken from the peak in the tan(δ) data, which more closely corresponds to a relaxation mid-point temperature. At this temperature, there is already significant molecular motion occurring. A second relaxation temperature can be defined by the peak of the loss modulus, E". This temperature is more representative of the relaxation on-set temperature. Unless otherwise stated, relaxation temperatures referred to in this work will be taken from the1.0 Hz tan(δ) peak.

The α-relaxation has been shown to have a high dependence on the strength of interactions between the $-SO_3^-$ groups of the polymer side-chains, with the α-relaxation temperature, T_α, occurring around 115°C for the Nafion® 212 used in this study, and is in good agreement with literature values[41-44]. Additionally, the α-relaxation involves significant, cooperative motion of polymer chains resulting in the T_α being heavily influenced by the mechanical energy input frequency[45]. This is clearly seen by the shift in tan(δ) peak to higher temperature as frequency increases from 0.1Hz to 10Hz (Figure 2.4a).

The β-relaxation is challenging to observe in Nafion®, and is seen here as a small peak in E", and a step in tan(δ). Work done by *Moore et. al.* has shown that this transition is likely the true-glass transition, T_g, of Nafion®, where the relaxation is primarily caused by motion of the backbone main-chain within the static hydrogen-bonded network of SO_3^- end groups[41, 42]. Here we observe a β-relaxation temperature, T_β, occurring between 5 and 10°C. Association of this relaxation with a glass transition is also supported by the T_g step behavior of the T_2 transition observed in the DSC trace of N212 near 0°C from the previous section (Figure 2.3).

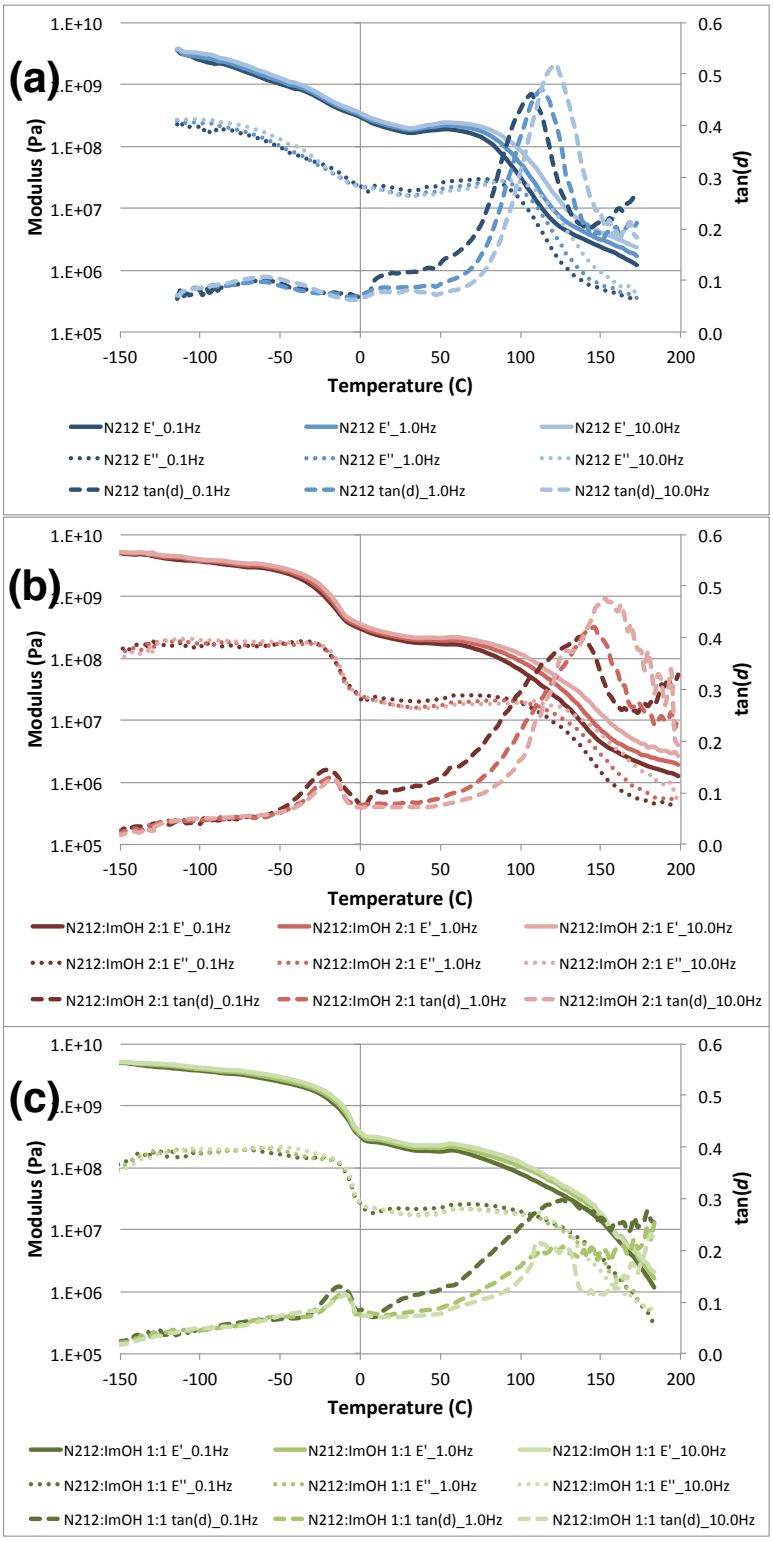

Figure 2.4: Dynamic mechanical E' (—), E" (···), tan(δ) (---) vs temperature plots of N212 (a), N212:ImOH 2:1 (b), and N212:ImOH 1:1 (c) measured at 0.1, 1.0, and 10Hz.

Table 2.2: Summary of relaxation temperatures as determined by E" and tan(δ).

N212	α (°C)		β (°C)		γ (°C)	
	E"	tan(δ)	E"	tan(δ)	E"	tan(δ)
0.1Hz	76	107	~ 4	~ 8	-112	-59
1.0Hz	85	113	—	—	-105	-59
10.0Hz	92	122	—	—	-100	-59
N212:ImOH 2:1						
0.1Hz	71	138	~ 11	~ 11	-35	-22
1.0Hz	90	146	—	—	-33	-20
10.0Hz	110	153	—	—	-37	-17
N212:ImOH 1:1						
0.1Hz	66	126	~ 25	~ 25	-23	-13
1.0Hz	63	113 - 131	—	—	—	-10
10.0Hz	60	110 - 131	—	—	—	-10

The γ-relaxation of N212 is seen as a broad peak in the tan(δ) centered around -59°C. In the literature, this relaxation is attributed to localized motion of the fluorocarbon (-CF_2-) backbone[41, 46]. Relaxation temperatures as determined by E" and tan(δ) are summarized in Table 2.2.

DMA data for N212:ImOH 2:1 is shown in Figure 2.4b. Here we see that the addition of ImOH in the 2:1 ratio has little effect on the starting and ending modulus, with E' decreasing from 5.0 x10^9 to 2.0 x10^6 Pa over the observed temperature range. However, the low temperature E' of the 2:1 membrane is more stable than the N212 below -20°C. This corresponds with an increase in the γ-relaxation temperature from -59°C for N212 to -20°C for N212:ImOH 2:1, as well as a decrease in the temperature range over which the relaxation occurs (indicated by the sharpening of the tan(δ) peak). A β-relaxation is still observed between 5 and 10°C in the 0.1 Hz tan(δ) data, but has decreased in intensity as compared with N212. The addition of ImOH in a 2:1 ratio greatly affects the α-relaxation, where we see a shift in T_α to about 145°C, as well as broadening of the tan(δ) peak and decrease in the relaxation intensity.

The DMA data for N212:ImOH 1:1 is shown in Figure 2.4c. Once again we see that the addition of ImOH has little effect on the storage modulus, with E' for the 1:1 membrane decreasing from 5.0 x10^9 to 1.7 x10^6 Pa over the temperature range observed. As with the 2:1 membrane, the low temperature modulus of N212:ImOH 1:1 remains stable until about -10°C, at which point there is a sudden decrease in E' corresponding to the γ-relaxation. A β-relaxation is once again observed in the 0.1 Hz

tan(δ) data only, but the step in tan(δ) has broadened and T_β has shifted to about 20°C. The T_α occurs at approximately 125°C, which is between the α-relaxation temperatures of the N212 and N212:ImOH 2:1 membranes. Additionally, the α-relaxation peak has further broadened and decreased in magnitude.

From the DMA data, we see that the addition of ImOH into the Nafion® structure has a significant, and complex, effect on the mechanical properties of the membrane. In both ImOH modified membranes, the relaxation temperatures of the α- and β-relaxations are increased suggesting that the addition of ImOH has a stiffening effect on the polymer structure. The increase in T_α, broadening of the tan(δ) peak, and decrease in relaxation intensity, are characteristics typically associated with cross-linking polymers[45]. However, the addition of ImOH also increases both the T_γ and γ-relaxation peak intensity, an effect typical of the plasticization of amorphous polymers[45]. The coexistence of these two effects suggests that ImOH influences the Nafion® backbone differently than the side chain. ImOH appears to have a cross-linking like effect on the SO_3^- end group network, resulting in the observed effects on the α- relaxation, while allowing for increased localized motion of the fluorocarbon backbone through plasticization, as demonstrated by the changes in the γ-relaxation.

2.3 Conclusions

Nafion® 212 membranes were modified with 4(5) hydroxymethyl imidazole (ImOH) in order to produce membranes with acid:base ratios of 2:1 and 1:1. Proton and fluorine NMR measurements showed that the nature of the bonding interaction between the ImOH and the SO_3^- end groups is dependent upon the amount of ImOH added, such that the desired ester formation is only present in the 2:1 membrane. Using a 1:1 ratio resulted in the formation of a salt.

Thermal properties measurements showed that the addition of ImOH to the Nafion® structure decreases membrane water up-take from the air and increases the onset temperature of thermal desulfonation, improving thermal stability. Additionally, differences in thermal transition behavior between the 2:1 and 1:1 membranes, as studied by DSC, support the difference in N212:ImOH bonding structures determined by NMR.

DMA showed that the addition of ImOH to Nafion® has a complex effect on the mechanical properties. While the storage modulus of the membranes remains relatively unchanged over the temperature range studied, there is a considerable effect on the temperature and behavior of the thermal relaxations. The ImOH modified membranes exhibited an increase in α-relaxation temperature typical of cross-linked polymers, while increased γ-relaxation intensity suggests the plasticization of the fluorocarbon backbone.

Considering the thermal and mechanical properties studied, we can conclude that the nature of the bonding interaction between ImOH and the PFSA has significant, and complex effects on membrane properties. However, the sensitivity of stable ester bond formation on the acidic environment within the membrane, makes the N212:ImOH 2:1 membrane of most relevance to this study.

Chapter 3

Water Up-take, Ionic Conductivity, and Swelling of Polymer Electrolyte Membranes

3.1 Introduction

The high proton conductivity of Nafion® is strongly dependent on the water swollen, phase-separated network of ionic-domains[1, 3, 7]. While this network of water channels provides a pathway for fast proton transport through the membrane via the structural diffusion of water, it also results in a variety of negative properties, such as excessive swelling and high fuel crossover[4, 21]. Development of a membrane that uses a stationary proton solvent for proton transport with low dependence on water is desired, because removal of water from the membrane would eliminate electro-osmotic drag, a key contributor to methanol transport through the membrane.

Imidazole has been of particular interest as a proton solvent due to its ability to transport protons via structural diffusion similar to that of water. It is also apparent that imidazole must be tethered to the polymer structure in order to prevent it from washing out of the membrane during fuel cell operation[7, 26, 29]. The addition of 4(5)-hydroxymethyl imidazole to the PFSA structure of Nafion® results in the immobilization of imidazole via the formation of ester bonds between the hydroxyl group of imidazole and the sulfonic acid end groups of the Nafion® side chains (Section 2.2.1).

Since ImOH interacts with the SO_3^- end-groups that provide a pathway for water and proton transport through the membrane, it is important to understand how the presence of ImOH in the membrane affects these properties. TGA measurements in Section 2.2.2 have already showed that the ImOH modified membranes exhibit reduced water up-take in air. This chapter further investigates the membrane water up-take characteristics, as well as the proton conductivity and swelling behavior of N212 membranes modified with ImOH.

3.2 Discussion

3.2.1 Water Up-take

Experimental procedures for water up-take measurements performed by dynamic vapor sorption (DVS) are described in Section 6.2.1.

Nafion® 212 (N212) membranes were obtained and modified with 4(5)-hydroxymethyl imidazole (ImOH), as discussed in Section 6.1.1, to have acid:base ratios of 1:1 and 2:1. Water up-take measurements were performed at 50°C by cycling relative humidity (RH) from 0% to 95% to 0%. Figure 3.1 shows the typical moisture sorption and desorption kinetic results obtained. Specifically, Figure 3.1a is the sorption/desorption results for N212 at 50°C. The dotted line shows the sample chamber humidity versus time on the right axis, while the solid line shows the percent change in mass, with reference to the dry mass, versus time on the left axis. The sample mass increases and decreases with the corresponding changes in RH and quickly reaches equilibrium.

From the equilibrium values at each RH step, the isothermal sorption/desorption behavior can be determined and is shown in Figure 3.1b. The sorption cycle is shown by the solid line, and the desorption cycle is shown by the dotted line. From this cycle it

can be seen that water sorption is a reversible process wherein all the water that enters the membrane during sorption is lost during desorption, returning the sample to its original dry mass. This result is in agreement with the work done by *Burnett et al.*[47] The shape of the isotherm is characteristic of a sorbent material that undergoes unrestricted monolayer-multilayer sorption. In Figure 3.1b, the beginning of the linear portion of the isotherm, point *B*, is generally considered to represent the completion of monolayer coverage and the beginning of multilayer sorption[48].

Additionally, at high humidities, there is a measurable hysteresis between the sorption and desorption isotherms. The appearance of hysteresis loops is typically associated with capillary condensation within the mesoporous structure, and in Nafion® this is observed as a decrease in water diffusion through the membrane at higher humidities[47-49]. The change in water dynamics with increasing humidity can be observed in Figure 3.2 where the water-sorption curve from Figure 3.1a has been reproduced and normalized in order to compare select humidity steps. The sample reaches an equilibrium state in the lower humidities (<50%RH) in as little as 10 minutes. Continuing to higher humidities results in increased equilibrium times suggesting slower water diffusion kinetics, which will be discussed in more detail later in this section.

Repeating water uptake measurements for the N212:ImOH 2:1 and 1:1 membranes results in similar kinetic sorption/desorption curves (not shown). Comparison of membrane water content is done using membrane λ *values*. The combined 50°C isothermal water content (λ) of N212 , N212:ImOH 2:1 and N212:ImOH 1:1 are shown in Figure 3.3. Here, it is clear that the addition of ImOH to the membrane reduces the water uptake of the membrane at all humidities, with water content at 95%RH dropping from λ = 9.2 for N212 to λ = 7.3 and 4.3 for N212:ImOH 2:1 and N212:ImOH 1:1 respectively.

During the sorption-desorption cycle, all membranes exhibit similar isothermal behavior. However, upon close inspection, a couple of differences in sorption behavior are observed. First, N212 exhibited a slope change at point B, around 10%RH. As ImOH content is increased to 2:1, then 1:1, the prominence of this slope change decreases, then vanishes. Taking this point to represent the transition between monolayer and multilayer sorption behavior, the disappearance of this transition suggests that the ImOH present in the membrane may be taking the place of water as the monolayer sorbate, allowing water to exhibit multilayer sorption behavior even at very low RH. This is apparent from the N212:ImOH 1:1 isotherm, which shows linear sorption behavior starting at 0%RH.

A second difference in isothermal behavior can be seen in the sorption hysteresis. N212 underwent reversible water uptake and exhibited a hysteresis loop at high humidity before returning to the original dry mass after all the water has desorbed. However, the ImOH modified membranes undergo irreversible sorption with a hysteresis loop that persists at low RH (Figure 3.4).

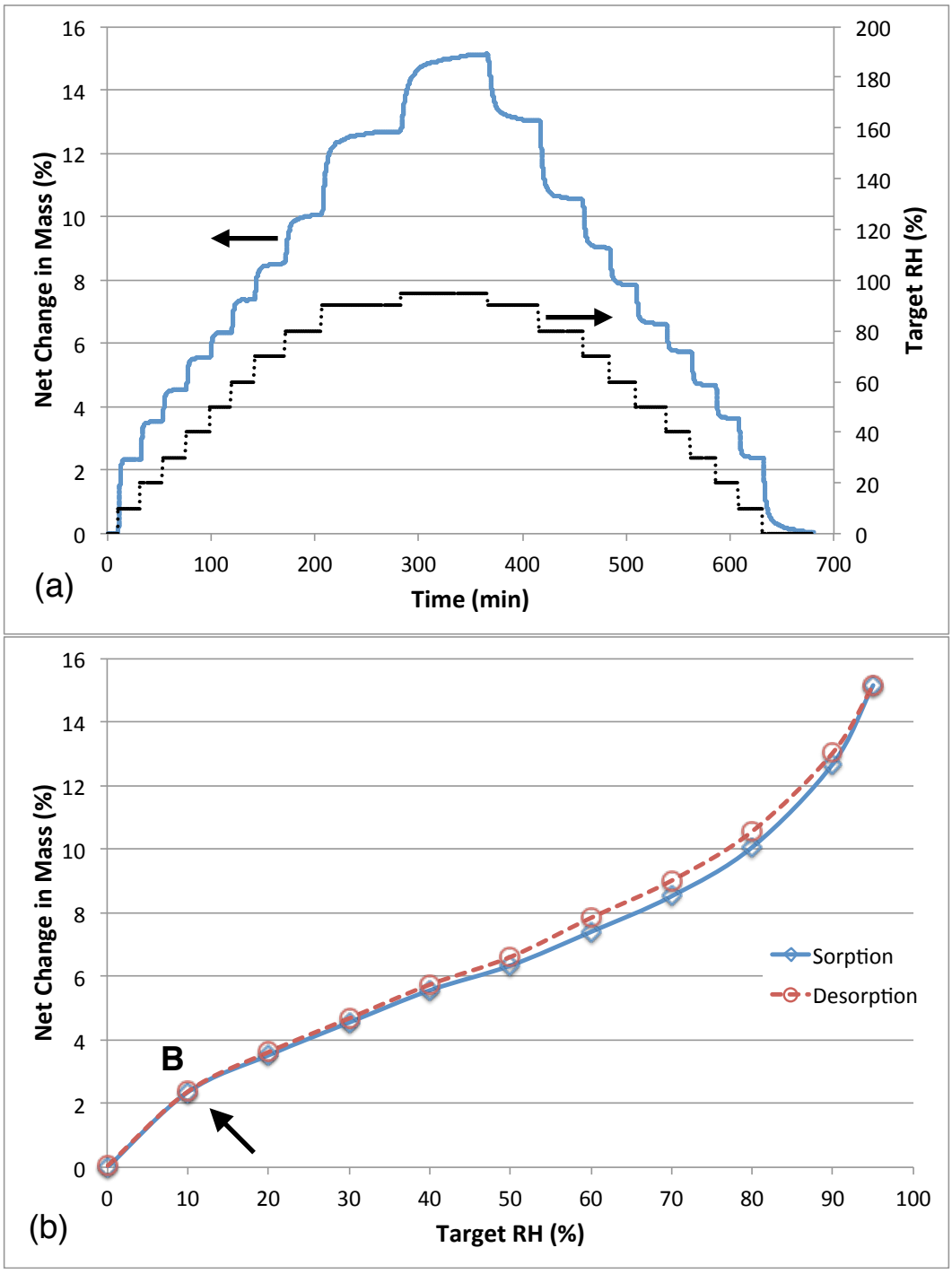

Figure 3.1: Water sorption and desorption kinetics (a) and isotherm (b) of N212 at 50°C. Water sorption kinetics a relatively fast as indicated by the rapid increase in mass with each change in humidity.

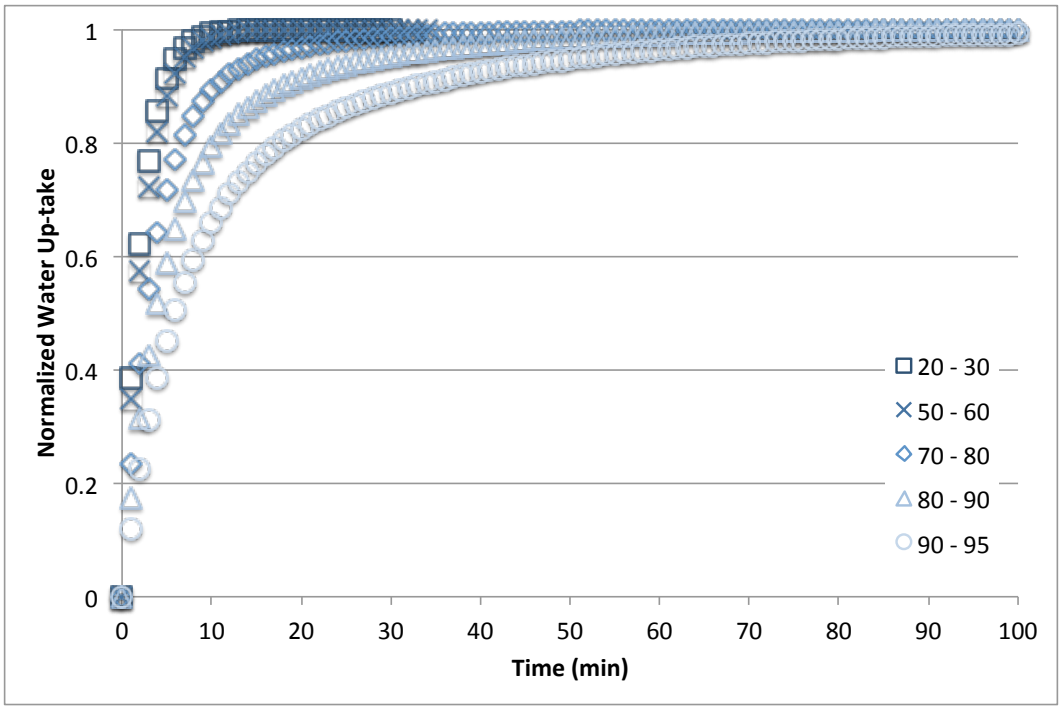

Figure 3.2: Normalized kinetic sorption data for N212 at 50°C.

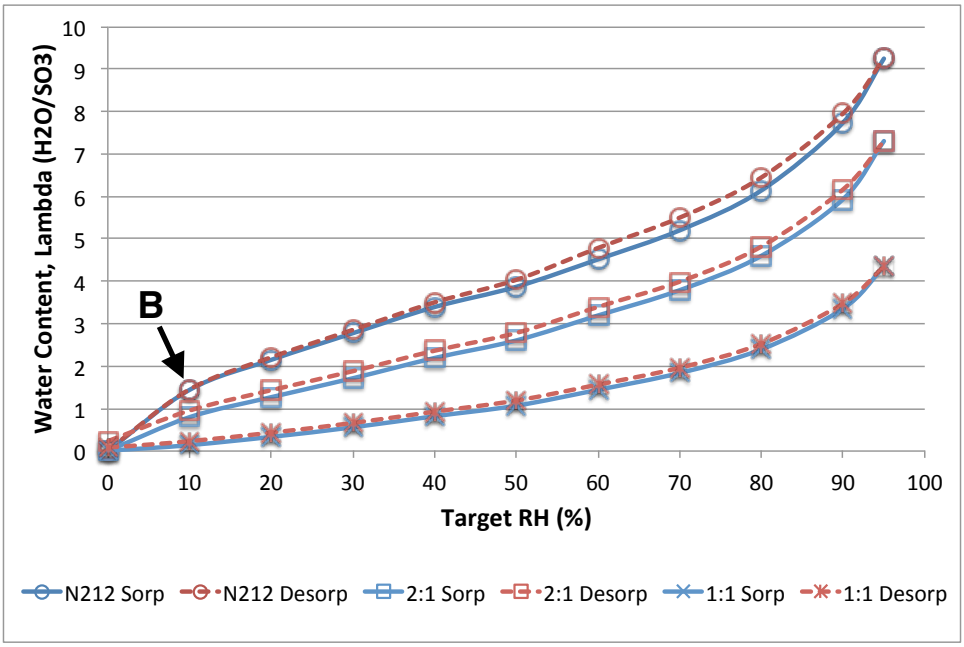

Figure 3.3: Isothermal sorption and desorption at 50°C of N212 (○), N212:ImOH 2:1 (□), and N212:ImOH 1:1 (✳). The addition of ImOH to N212 membranes reduces water uptake at all humidities.

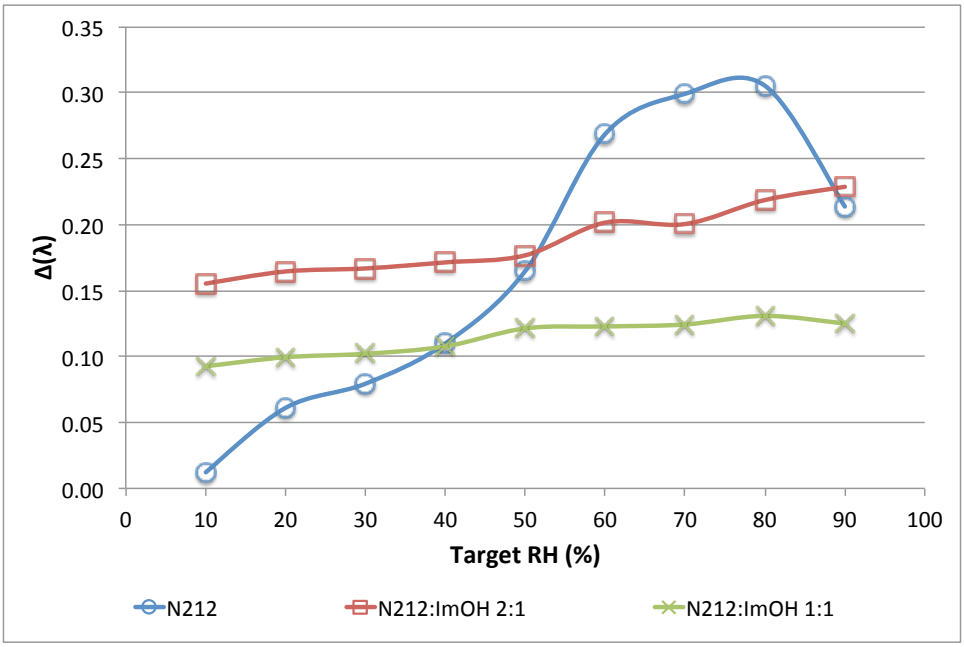

Figure 3.4: Difference in λ between sorption and desorption cycles showing membrane sorption-desorption hysteresis at 50°C of N212 (○), N212:ImOH 2:1 (□), and N212:ImOH 1:1 (✳).

Kinetic water sorption data from the modified membranes showed that the ImOH membranes exhibit similar kinetic sorption behavior as the unmodified N212 (Figure 3.2). Using the kinetic data, calculation of the inverse time constant, k_s, can be done for each RH step using Eq. 6.2, as described in Section 6.2.1. Membrane water-sorption dynamics are presented in Figure 3.5, which shows the rate constant as a function of water content, λ. Presented in this way, we see that for a given $\lambda > 2$, the rate of sorption is lower for ImOH modified membranes, showing that water transport into the ImOH modified membranes is slower than that of the unmodified N212.

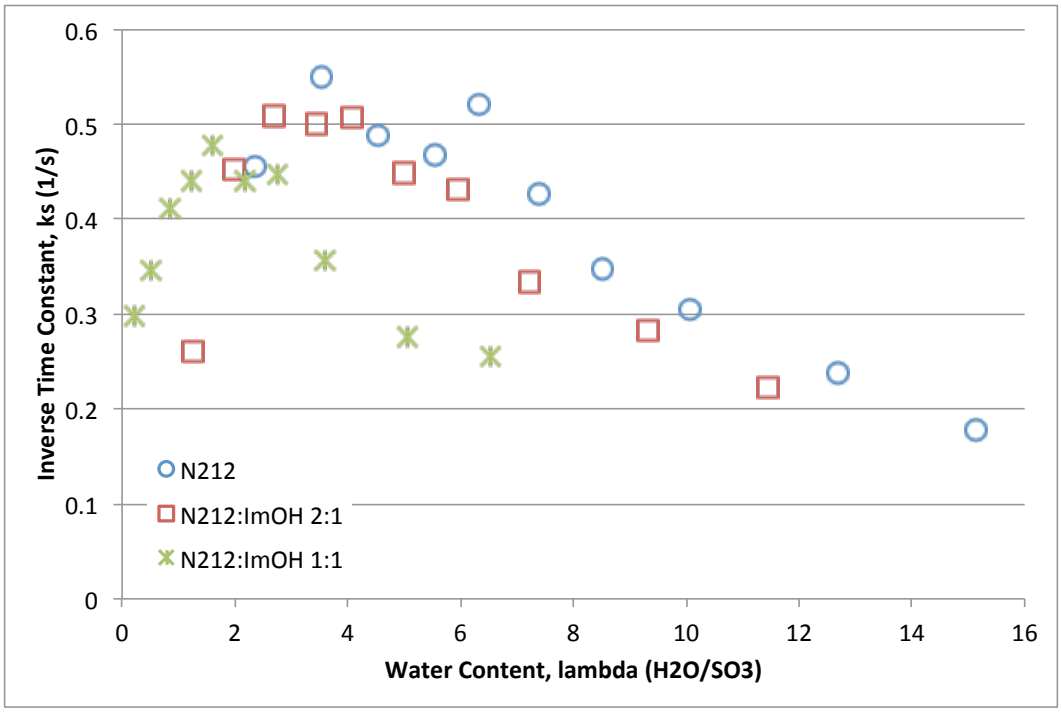

Figure 3.5: Rate constants for water uptake as a function of relative humidity at 50°C for N212 (○), N212:ImOH 2:1 (□), and N212:ImOH 1:1 (✳).

3.2.2 Ionic Conductivity

Membrane proton conductivity was measured through the plane of the membrane using a four-terminal AC impedance spectroscopy method described in Section 6.2.2. Isothermal humidity scan experiments were performed at 50°C to observe the effects of relative humidity on proton conductivity. Impedance spectra obtained for N212 are shown for select humidities in Figure 3.6. It is clear from the complex impedance loops that Nafion® exhibits both low and high frequency dependence on RH. The low frequency resistance is the sum of the ohmic resistance of the membrane as well as the charge transfer resistance within the electrodes, and the RH dependence is evidenced by the decrease in the low frequency arc with increasing RH (Figure 3.6 top)[51].

In this section we will be focusing on the high frequency region, as it is the high frequency resistance, R_{HF}, that is a result of the bulk membrane resistance. Humidity dependence of R_{HF} is seen as a shift in the high frequency intercept to lower Z' values (Figure 3.6 bottom)[51, 52]. Determination of R_{HF} was done by analyzing the impedance data using ZView software (Scribner Associates, Inc) and the equivalent circuit model shown in Figure 3.7. The R_{HF} values obtained through circuit modeling were used to calculate membrane proton conductivity, σ, using Equation 6.3.

Isothermal humidity scans at 50°C were performed on N212, N212:ImOH 2:1, and N212:ImOH 1:1 and R_{HF} values were obtained. The calculated conductivities are shown in Figure 3.8 as a function of relative humidity (a) and water content, λ, (b). From Figure 3.8a, there is a clear dependence of conductivity on relative humidity for N212 as seen by the exponential increase in conductivity as humidity is increased from 4.5 $x10^{-3}$ S/cm at 20%RH to 9.0 $x10^{-2}$ S/cm at 95%RH. This exponential RH dependence is exhibited by all three membranes. However, the addition of ImOH to the membrane reduces membrane conductivity at all humidities, with the N212:ImOH 2:1 and 1:1 being reduced from 9.0 $x10^{-2}$ S/cm at 95%RH to 2.2 $x10^{-2}$ and 1.4 $x10^{-3}$ S/cm respectively. Figure 3.8b shows the conductivity data replotted as a function of water content. From this we see that the addition of ImOH also reduces proton conductivity for a given λ, meaning there is less conductivity per water molecule in the membrane.

It has been shown in various studies, that the proton conductivity of PEMs exhibits a temperature dependence that can be described using an Arrhenius plot wherein conductivity increases with increasing temperature[4, 53-55]. In this study, conductivity was measured over the temperature range of 30°C to 120°C at 50% and 95%RH, as described in Section 6.3.2, and revealed that the ImOH modified Nafion® maintained the Arrhenius behavior allowing for comparison of energy of activation for proton conduction using the Arrhenius equations

$$\sigma = \frac{A}{T}\exp\left(-\frac{E_a}{RT}\right) \qquad [3.1]$$

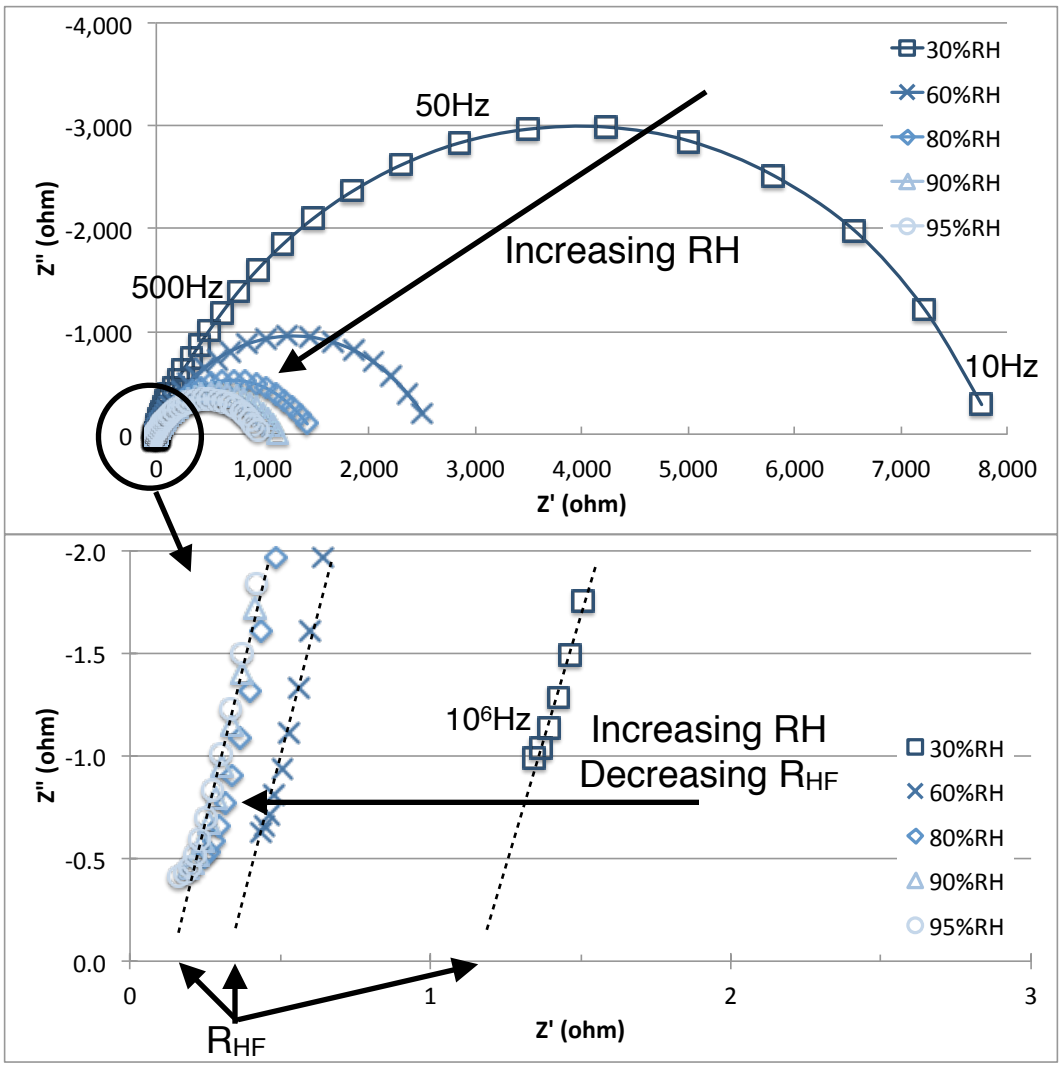

Figure 3.6: Complex impedance spectra of N212 at select relative humidities. Low frequency humidity dependence is seen by the decrease in low frequency impedance loop (top). High frequency humidity dependence is seen as a shift in the high frequency intercept to lower R_{HF} values (bottom).

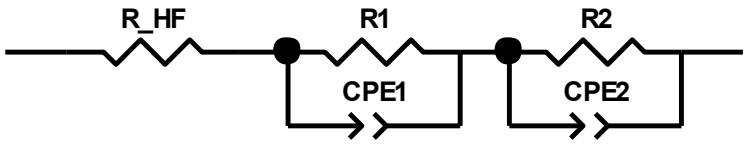

Figure 3.7: Equivalent circuit model used for determination of R_{HF}. CPE is a constant phase element used to account inhomogeneities in the flow of current on the electrodes.

$$\ln(\sigma T) = \ln(\sigma_0) - \frac{E_a}{R}\left(\frac{1}{T}\right) \qquad [3.2]$$

where σ, σ_0, E_a, R, and T are the membrane conductivity (S cm^{-1}), the pre-exponential factor (S K^{-1} cm^{-1}), the proton conducting activation energy (kJ mol^{-1}), the ideal gas constant (J mol^{-1} K^{-1}), and temperature (K), respectively. From Equation 3.2, the plot of $ln(\sigma T)$ versus $1/T$ (Figure 3.9) allows for the determination of E_a and $ln(\sigma_0)$. The values obtained for each membrane are shown in Table 3.1 where it can be seen that the addition of ImOH to Nafion® has a significant effect on the activation energy for proton conduction. At 50%RH, proton conduction in the N212:ImOH 2:1 membrane requires almost 2.5 times the energy as in N212, and N212:ImOH 1:1 requires nearly 5 times the energy as in N212. Increasing the RH to 95%, we see that E_a of the ImOH modified membranes has a strong dependence on relative humidity, and the energy required to conduct protons decreases at higher humidity, while the E_a of N212 remains relatively unchanged. This dependence in RH results in the N212:ImOH 2:1 membrane having a similar E_a to that of N212 at 95%RH. However, despite requiring the same energy to conduct protons, the magnitude of conductivity is lower at all temperatures for the N212:ImOH 2:1 membrane.

Conductivity measurements have shown that the addition of ImOH to the Nafion® structure reduces proton conductivity for all the temperature and humidity conditions tested. The ImOH modified membranes also demonstrate reduced conductivity for a given water content. What is important to note is that, at 95%RH, N212:ImOH 2:1 requires about the same amount of energy for proton conduction to occur as the unmodified N212, despite having lower overall conductivity. With proton conduction requiring the same activation energy, yet resulting in different conductivities, this suggests that there is another factor influencing membrane conductivity.

Table 3.1: Proton conducting activation energies and pre-exponential factors for N212 based membranes at 50% and 95%RH in the temperature range of 30°C to 120°C.

Sample	50%RH		95%RH	
	E_a [kJ mol^{-1}]	$\ln(\sigma_0)$ [S K^{-1} cm^{-1}]	E_a [kJ mol^{-1}]	$\ln(\sigma_0)$ [S K^{-1} cm^{-1}]
N212	13.3	6.98	19.1	10.1
N212:ImOH 2:1	30.5	9.73	17.4	8.41
N212:ImOH 1:1	59.4	17.5	35.2	12.2

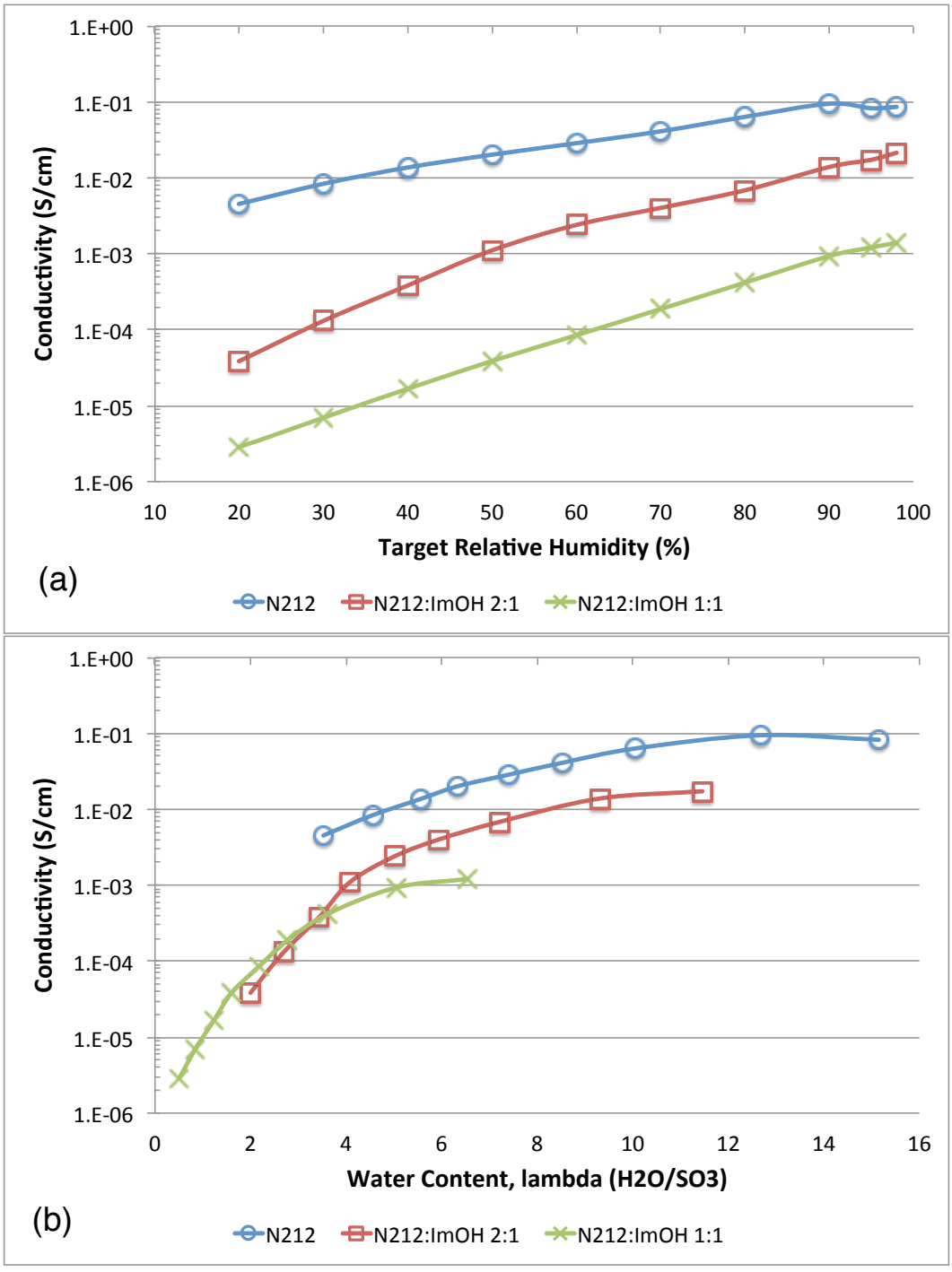

Figure 3.8: Isothermal through-plane proton conductivity at 50°C of N212 (○), N212:ImOH 2:1 (□), and N212:ImOH 1:1 (✳) as a function of relative humidity (a), and membrane water content (b).

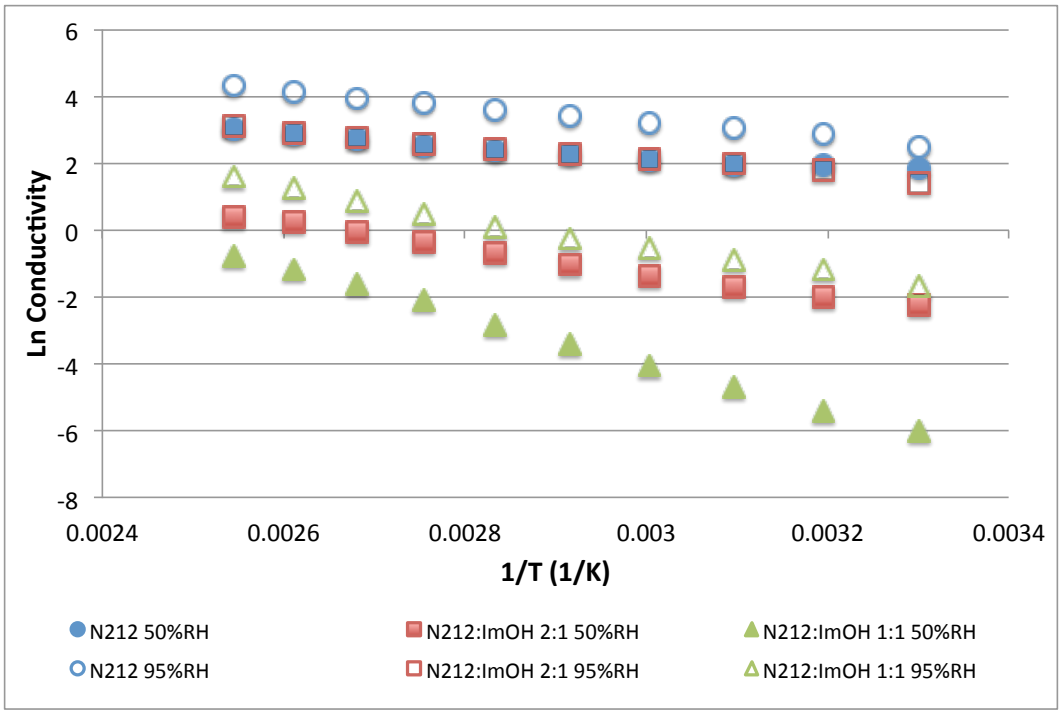

Figure 3.9: Arrhenius plot showing temperature dependence of proton conductivity N212 (○), N212:ImOH 2:1 (□), and N212:ImOH 1:1 (✳) at 50% and 95%RH.

3.2.3 Morphology

Membrane morphology was investigated using small angle X-ray scattering (SAXS) under varying humidity conditions to observe the effects of ImOH on the nanostructure of Nafion®. Measurements were performed on the N212 and N212:ImOH 2:1 membranes at 50°C under 50, 75, 85, 90, and 95%RH using the method described in Section 6.3.3.

Scattering curves for N212 at each humidity step are shown in Figure 3.10. Curves shown were obtained at each RH step after the sample was equilibrated for 1h. Two peaks are observed in the scattering vector, *q*, range shown. The left peak, observed between q = 0.04 and 0.08 $Å^{-1}$, is the *matrix knee* and is attributed to the distance between crystalline domains of the polymer matrix. The right peak, between q = 0.12 and 0.23 $Å^{-1}$, is the *ionomer peak* and corresponds to the spacing between water domains within the polymer matrix.[56-59]

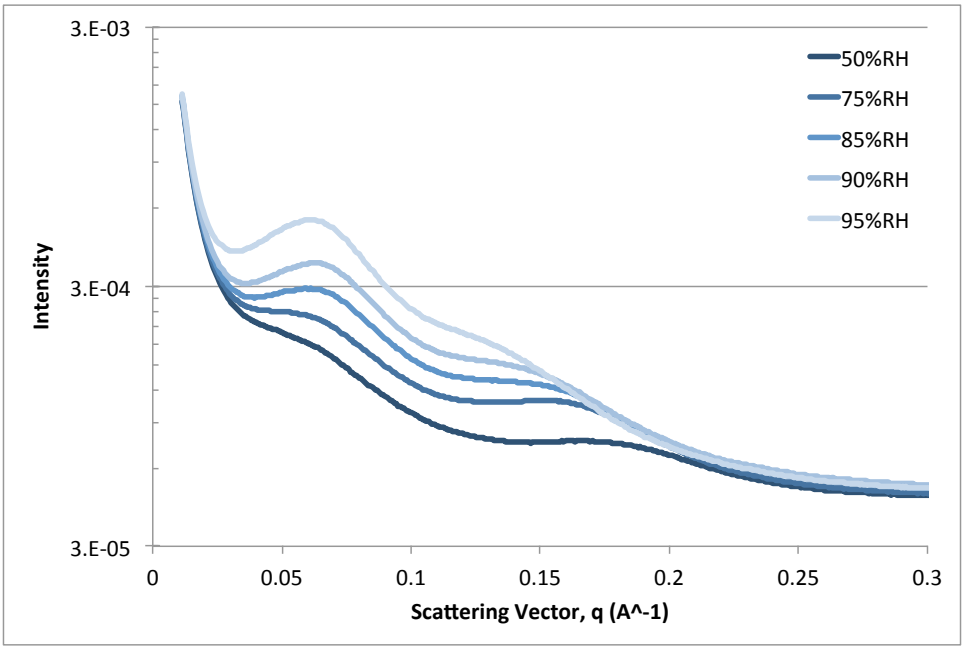

Figure 3.10: Scattering curves for N212 equilibrated under different humidities at 50°C.

From Figure 3.10, it is clear that as RH is increased there is a change in the morphology of the membrane. Increased humidity causes a slight shift in the matrix knee to lower q values, indicating swelling from 0.066 $Å^{-1}$ (9.5 ± 1 nm) at 50%RH to 0.061 $Å^{-1}$ (10.4 ± 1 nm) at 95%RH. This shift is accompanied by peak sharpening indicating a narrowing of the distribution of states that contribute to scattering along this angle. Swelling effects are more apparent in the ionomer peak, where peak location shifts from q = 0.17 $Å^{-1}$ (3.8 ± 1 nm) at 50%RH to 0.12 $Å^{-1}$ (5.2 ± 1 nm) at 95%RH. However, the breadth of the ionomer peak makes determination of exact location difficult.

Humidity measurements were repeated for the N212:ImOH 2:1 membrane and revealed a similar swelling behavior to N212. Scattering curves for 50% and 95%RH are shown for both membranes in Figure 3.11, where we see that the matrix knee of N212:ImOH 2:1 remains very broad at 95%RH, and does not sharpen or increase in intensity as observed for the N212. The persistence of a broad matrix knee may be a result of the ImOH disrupting the backbone crystallinity in the 2:1 membrane, which would be consistent with DSC and DMA results discussed in Chapter 2.

A shift is observed in the ionomer peak of N212:ImOH 2:1 from q = 0.19 $Å^{-1}$ (3.3 ± 1 nm) at 50% RH to 0.17 $Å^{-1}$ (3.8 ± 1 nm) at 95%RH. That is, the hydrophilic domains of the N212:ImOH 2:1 membrane swell approximately 0.5 nm compared with the 1.5 nm swelling observed in the unmodified N212. Swelling of the ionomer domains exhibit similar behavior to the macroscopic up-take of water shown in Figure 3.3. When the ionomer domain d-spacing is plotted against membrane water content, λ, as shown in Figure 3.12, a linear relationship is observed. This behavior is consistent with observations reported by Kusoglu *et. al.*[56]

From Figure 3.12, it is clear that there is a linear relation between ionomer domain d-spacing and membrane water up-take. However, the N212:ImOH 2:1 membrane undergoes less swelling per additional water molecule than the unmodified N212 resulting in the observed slope change. Additionally, the shape of the ionomer peak in Figure 3.11 is different for the two membranes. The ionomer peak of N212:ImOH 2:1 becomes more defined at high humidity, unlike that of N212, which remains very broad. These observed differences in ionomer peak shape and swelling behavior suggest a difference in morphology of the swollen membranes. The broad ionomer peak of the unmodified N212 is a result of a distribution of domain sizes associated with the well-connected water channel network of hydrated Nafion®[1, 56]. The addition of ImOH reduces the total water content of the membrane, as discussed in Section 3.2.1 (Figure 3.3), resulting in less swelling. The well-defined ionomer peak observed in N212:ImOH 2:1 suggests the hydrophilic network is not as well connected as in the unmodified N212. A poorly connected hydrophilic network would result in a more tortuous conductive pathway, with more dead ends, leading to the decrease in membrane conductivity observed in Section 3.2.2 (Figure 3.9).

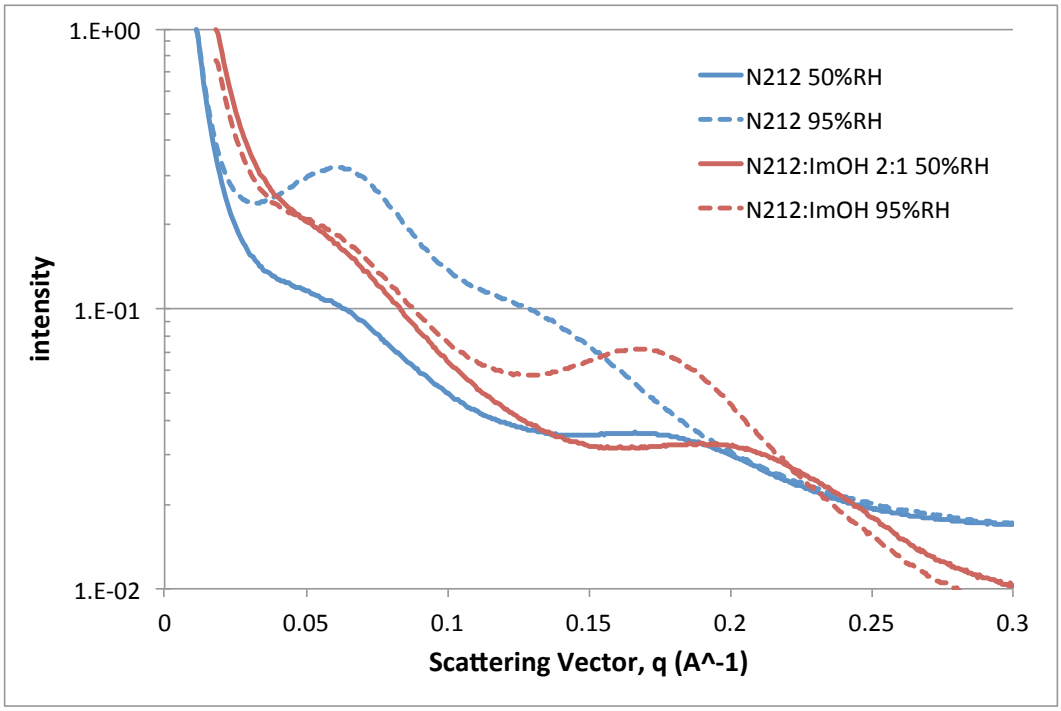

Figure 3.11: Scattering curves of N212 and N212:ImOH 2:1 equilibrated under 50% and 95%RH at 50°C.

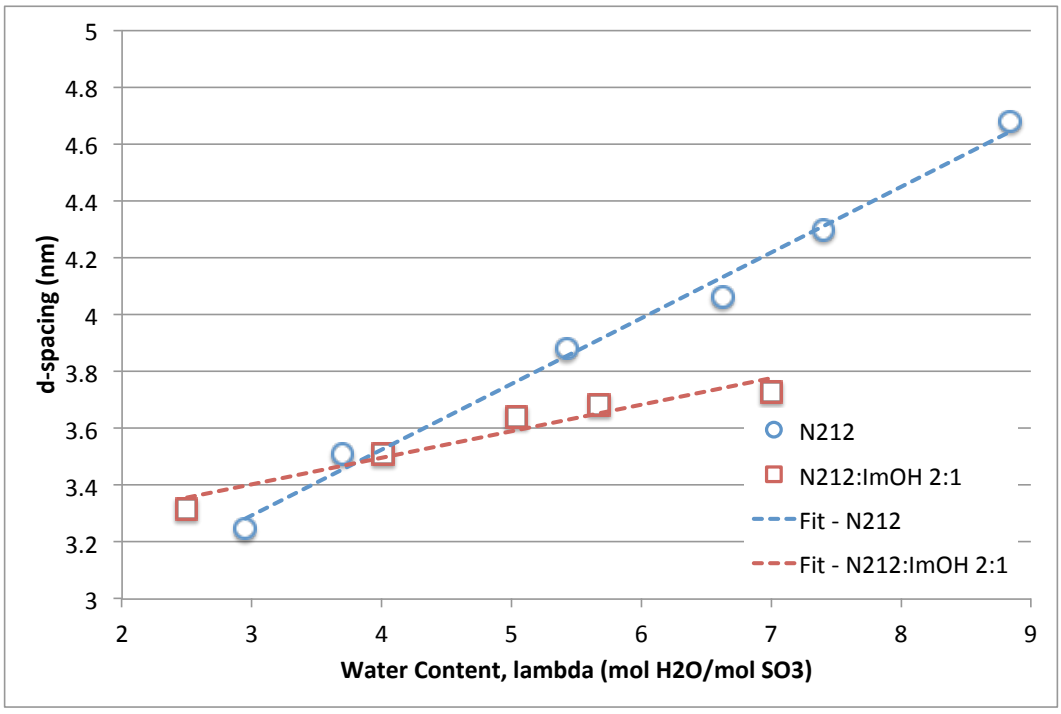

Figure 3.12: Domain *d*-spacing of N212 (○) and N212:ImOH 2:1 (□) as a function of membrane water content, λ, at 50°C.

3.3 Conclusions

Water sorption, proton conductivity, and morphology of Nafion® 212 membranes modified with ImOH were examined. DVS measurements showed that the addition of ImOH to the membrane structure reduces the amount of water sorbed into the membrane. Additionally, kinetic sorption data reveals that ImOH modification results in a decrease in the rate at which water moves into the membrane. It is expected that reduction of water diffusion kinetics in the membrane will result in increased selectivity by limiting electro-osmotic drag and diffusion effects. This will be examined further in the following chapter.

Proton conductivity was measured using a through-plane technique, and determined that modification of N212 with ImOH reduces membrane conductivity at all RH and water content. However, the Arrhenius behavior of the membranes allows for calculation of the proton conducting activation energy, E_a. This showed that, at 95%RH, the N212:ImOH 2:1 and unmodified N212 membranes require the same E_a for proton conduction to occur. The lower magnitude of conductivity is likely a result of a decrease in the quantity of charge carriers that results from the manor in which ImOH is attached to the Nafion® structure.

SAXS allowed for the study of swelling behavior of the membrane morphology. Observation of the ionomer domain revealed that the lower water sorption of N212:ImOH 2:1 corresponds to a reduction in swelling. Interestingly, total swelling of the ionomer domain was not only decreased by the addition of ImOH, but swelling per water molecule was also decreased. If we recall from Section 2.2.3, DMA measurements revealed that ImOH causes plasticization of the PTFE backbone structure. This, in addition to the large distribution of states indicated by the broad matrix knee in Figure 3.11, suggests that water in the ImOH modified membranes is not as restricted to the ionic domains as in the unmodified N212.

Chapter 4

Fuel Cell Testing

4.1 Introduction

Effects of ImOH modification on the thermal, mechanical, transport, and morphological properties of Nafion® 212 membranes have, to this point, been studied outside of the fuel cell environment. While important insight into the characteristics of ImOH modified membranes has been made via ex-situ study, it is also important to understand membrane behavior when inside the fuel cell environment.

The complexity of a fuel cell imposes significant demands on membrane materials, requiring that they continue to function as an efficient proton conductor while maintaining effective chemical and electrical separation between the anode and cathode, as well as being well connected and compatible with the electrocatalysts within each catalyst layer. When assembled together in a fuel cell, it is important that all components continue to function together simultaneously. Fuel cell testing is the most commonly used technique for evaluation of fuel cells and fuel cell components. From fuel cell testing, the relationship between cell voltage and current density can be studied. In this work, this relationship is studied via a controlled current technique. A schematic of a typical polarization curve that results from controlled current experiments was shown in Figure 1.5, and discussed in Section 1.3.2 of Chapter 1.

In addition to general fuel cell performance, impedances associated with the membrane electrode assembly (MEA) can be studied during fuel cell operation using electrochemical impedance spectroscopy (EIS). Ex-situ EIS measurements were discussed in Section 3.2.2, where AC impedance spectroscopy was used for the determination of proton conductivity in the bulk membrane. During fuel cell operation, EIS aids in the characterization of electrode-electrolyte interface behavior.

Linear sweep voltammetry (LSV) is also conducted during fuel cell testing. LSV is a technique used for measuring methanol crossover, in which methanol is electrochemically oxidized at the cathode resulting in a limiting current density, where current density is limited by the transport of methanol through the membrane[4, 21, 22].

In this chapter, N212:ImOH 2:1 and unmodified N212 membranes are assembled into MEAs and tested in direct methanol fuel cells in order to study how the properties of ImOH modified membranes, already observed ex-situ, behave in the fuel cell environment.

4.2 Discussion

4.2.1 Membrane Electrode Assembly

Membrane electrode assemblies (MEAs), with an active area of 5 cm^2, were constructed from N212:ImOH 2:1 and unmodified N212 membranes using the hot pressing technique described in Section 6.3.1. After hot pressing, the MEAs were allowed to cool to room temperature, and the electrodes were visually inspected for signs of delamination from the membrane prior to assembling into the fuel cell hardware.

4.2.2 Fuel Cell Testing

The MEAs were evaluated for their performance in a DMFC using cell polarization measurements outlined in Section 6.3.2. A series of polarization measurements were made over several hours to observe stability of cell operation. Figure 4.1 shows the resulting polarization curves for the unmodified N212 DMFC operating at 60°C.

An OCV of about 0.59V was observed for the duration of testing. From the polarization curve we can observe two of the main loss stages discussed in Section 1.3.2. Activation losses are evident from the steep initial loss in cell voltage below 20 mA/cm^2, from 0.59V at OCV to 0.47V at 20 mA/cm^2. Above 20 mA/cm^2, the cell voltage is decreasing due to ohmic losses largely resulting from MEA resistance. This continues until the maximum tested current density of 220 mA/cm^2. No mass transport loss region was observed at the current densities tested. Cell power density peaked at 31 mW/cm^2 with a cell voltage of 0.22V. Looking at the cell behavior over the 4 cycles shown, we see that there is a slight increase in cell performance from the 1st to the 4th cycles.

In Figure 4.2, the polarization curve for a DMFC using a N212:ImOH 2:1 MEA is shown. The OCV showed more fluctuation during testing, but averaged 0.60V for the duration of testing. The addition of ImOH to the MEA resulted in a larger voltage drop below 20 mA/cm^2, due to activation losses, from 0.60V at OCV to 0.34V at 20 mA/cm^2, about double the loss as compared with the N212 MEA.

Above 20 mA/cm^2, in the ohmic loss region, the N212:ImOH 2:1 cell voltage decreases quickly, such that the maximum current density of the cell was 99 mA/cm^2 with a peak power density of 12 mW/cm^2 at 0.22V. Over the duration of the 4 cycles, cell performance decreased by almost 50% with maximum current dropping to 59 mA/cm^2 and peak power to 6 mW/cm^2 a 0.15V.

Looking closely at how the shape of the polarization curve changes from the 1st to the 4th cycle (Figure 4.2), we can see that the activation loss region increases and persists to higher current densities with each cycle. By the 4th cycle, the cell appears to be under activation loss for the duration of the cycle.

For comparison, the 1st cycle for each cell is reproduced in Figure 4.3. Here we can easily see the differences in cell behavior between the two cells.The addition of ImOH to the N212 membrane results in a significant decrease in cell voltage at low current densities due to activation losses. The decrease in cell voltage, due to activation losses of the N212:ImOH 2:1 MEA, is about double that of the N212 MEA, losing 0.26V and 0.12V respectively.

Above 20 mA/cm^2, both cells exhibit a change of slope indicating cell voltage is decreasing due to ohmic loss. Since the largest contributor to ohmic loss in the cell is the membrane, and conductivity measurements from Section 3.2.2 showed that the N212:ImOH 2:1 membrane has greater resistance, it is not surprising that the addition of ImOH to the membrane results in a steeper slope in the region. Impedance measurements from Section 3.2.2 showed that at 60°C the addition of ImOH to N212 resulted in an increase in membrane resistance of about 67%, while calculation of MEA resistance from the slope of the ohmic loss region (where $V = IR$) shows an increase in resistance of about 80% when ImOH is added. However, this is only a rough

comparison, because the ohmic loss region is influenced by many factors in addition to the membrane resistance.

From the polarization curves, it appears that one of the main contributing factors to the decrease in cell performance is related to electrode kinetics, as is evident from the increase in the activation loss region. EIS measurements performed while the cell is under load allow for further investigation into the factors effecting cell performance.

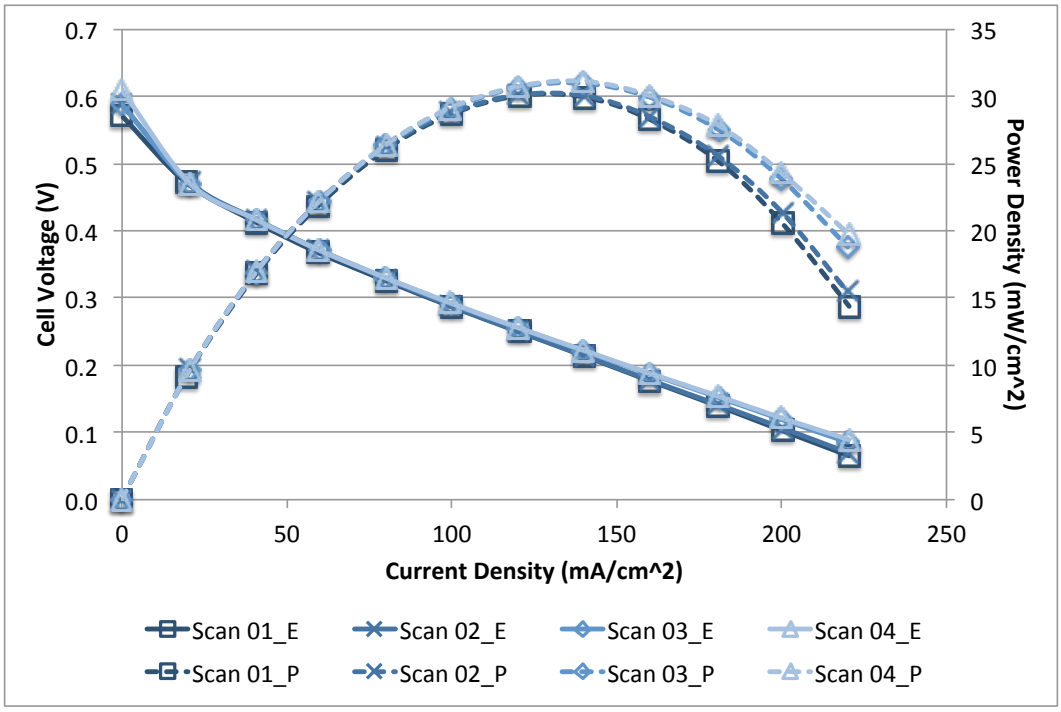

Figure 4.1: Polarization curves of an N212 DMFC operating at 60°C with 1M methanol fuel and oxygen cathode feed.

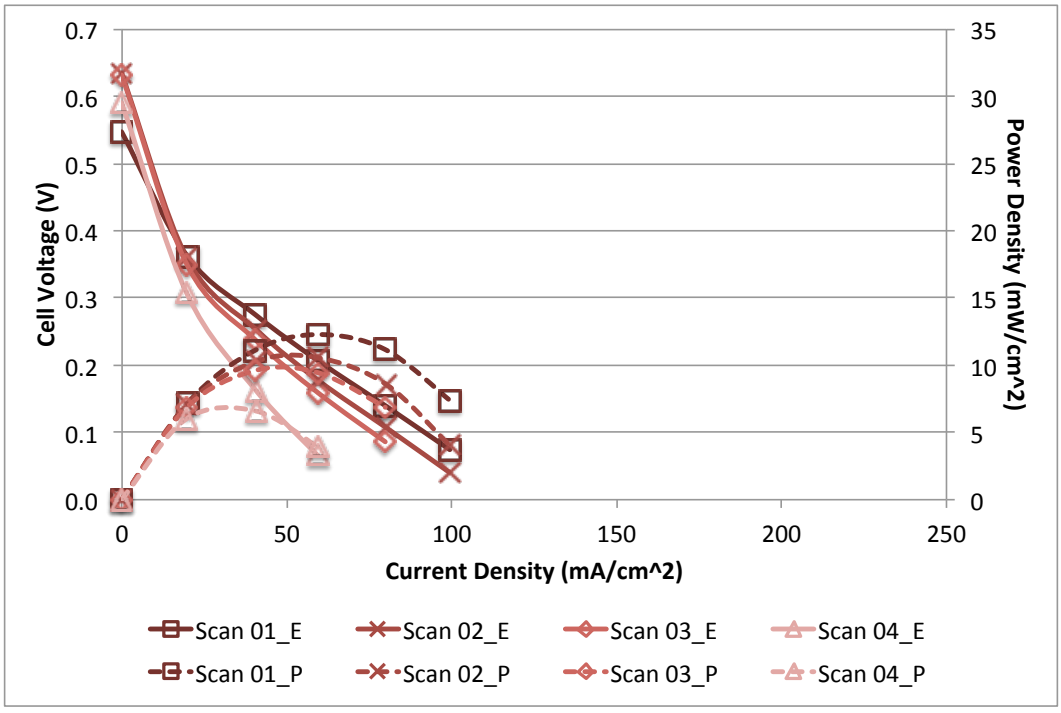

Figure 4.2: Polarization curves of an N212:ImOH 2:1 DMFC operating at 60°C with 1M methanol fuel and oxygen cathode feed.

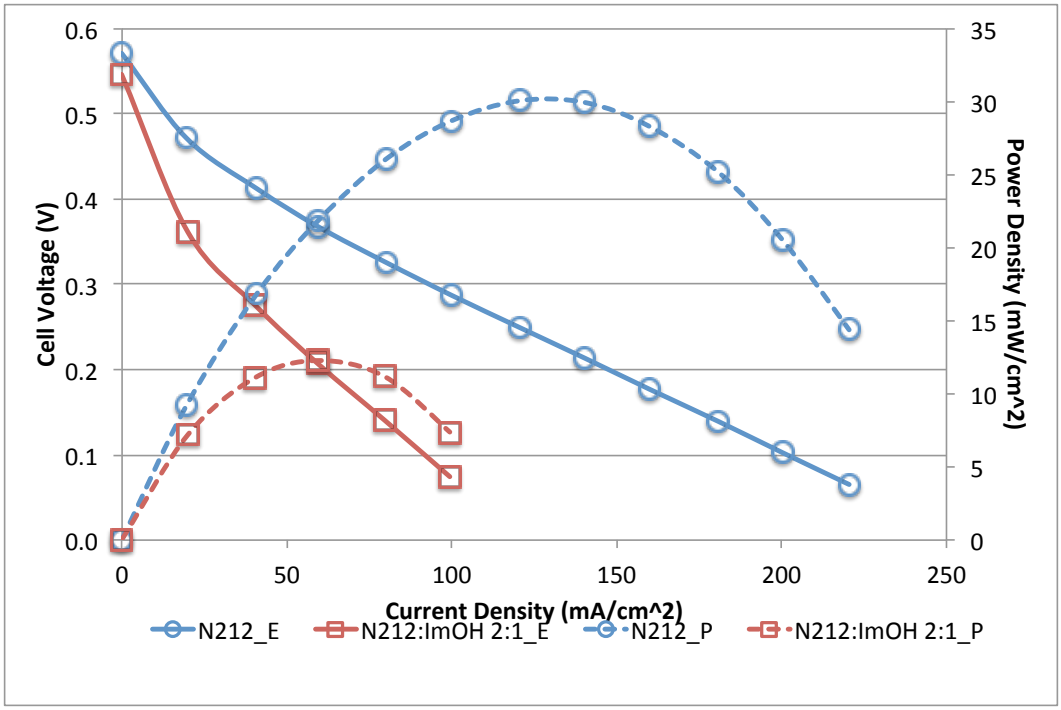

Figure 4.3: Comparison of first cycle polarization curves for N212 and N212:ImOH 2:1 MEAs in a DMFC operating at 60°C.

4.2.3 MEA Impedance

MEA impedance is measured while the fuel cell is under load using the electrochemical impedance spectroscopy (EIS) method described in Section 6.3.2. EIS measurements were taken at a variety of cell current densities. Figure 4.4. shows the Nyquist plot of a DMFC with N212 membrane operated at 60°C with a current density of 20 mA/cm^2. Two semicircles appear in the EIS spectrum, one at high-frequencies and one at low-frequencies. The low-frequency semicircle represents the mass transfer resistance of the reactants. The high-frequency semicircle represents the charge transfer resistance (R_{ct}) for the electrodes. The high frequency intercept of the EIS spectrum with the real axis (x-axis) is the ohmic resistance of the cell, dominated by the membrane resistance (R_{HF}).

Equivalent circuit modeling is used to simulate the charge transfer and mass transfer resistance values[62, 63]. However, study of mass transfer resistances is beyond the scope of this work. Simulation of charge transfer resistance and membrane resistance was done by fitting the high-frequency semicircle using the equivalent circuit model shown in Figure 4.5. In the model, R_{HF} is the ohmic resistance of the cell, R_{ct} is the charge transfer resistance of the electrodes, and CPE is a constant phase element used to account inhomogeneities in the flow of current on the electrodes. The model obtained from fitting the EIS spectra with the above equivalent circuit is shown in Figure 4.6.

EIS spectra for N212 and N212:ImOH 2:1 DMFCs operated at 60°C under select current densities are shown in Figure 4.7. Plotted on the same scale it becomes very clear that the addition of ImOH to the N212 membrane has a dramatic affect on the charge transfer resistance of the electrodes. This is indicated by the significant increase in the high-frequency semicircle of the N212:ImOH 2:1 DMFC. The EIS spectra for each cell were modeled with the equivalent circuit from Figure 4.5, and the simulated charge transfer (R_{ct}) and ohmic (R_{HF}) resistances are summarized in Table 4.1.

From the MEA impedance measurements, it is clear that the addition of ImOH to the N212 membranes has a significant effect on the electrodes. This effect is likely due to interactions between the nitrogen of the imidazole ring and the platinum catalysts in the electrode catalyst layers. It has been shown in the literature that imidazole will form complexes with platinum[60], and reduce catalytic activity[61].

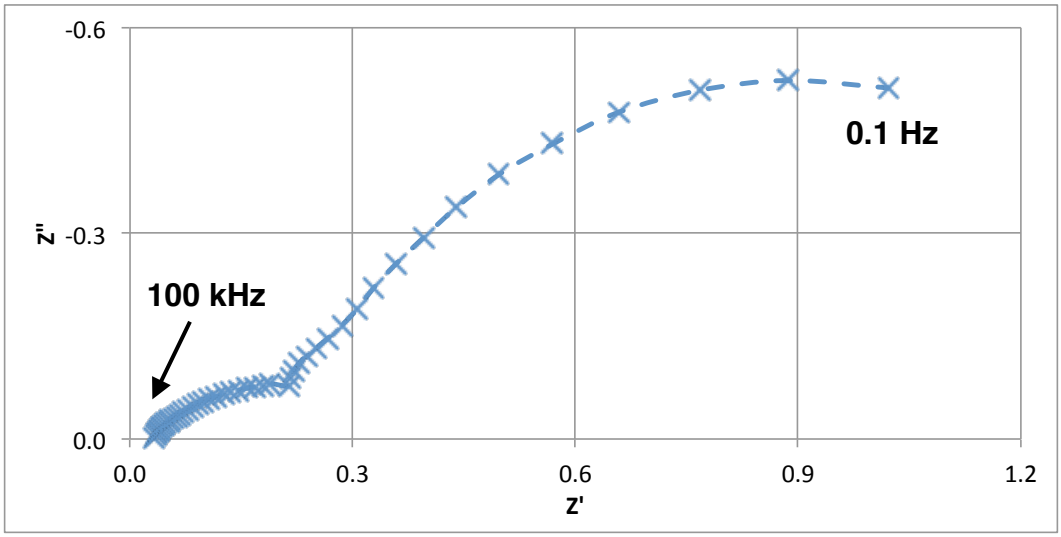

Figure 4.4: Nyquist plot of a DMFC with N212 membrane operated at 60°C with a current density of 20 mA/cm^2.

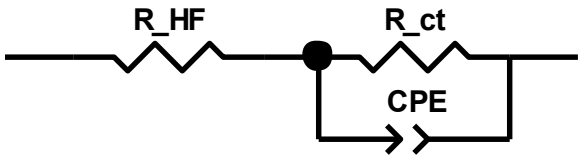

Figure 4.5: Equivalent circuit for EIS spectrum high-frequency semicircle modeling of DMFCs under load.

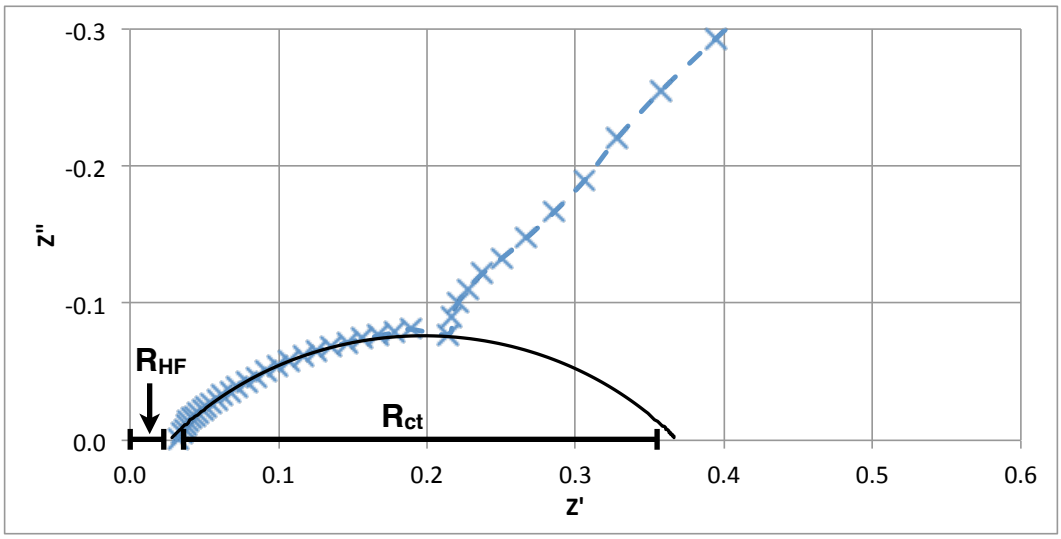

Figure 4.6: Nyquist plot of high-frequency semicircle with fit from equivalent circuit modeling of a DMFC with N212 membrane operated at 60°C with a current density of 20 mA/cm^2.

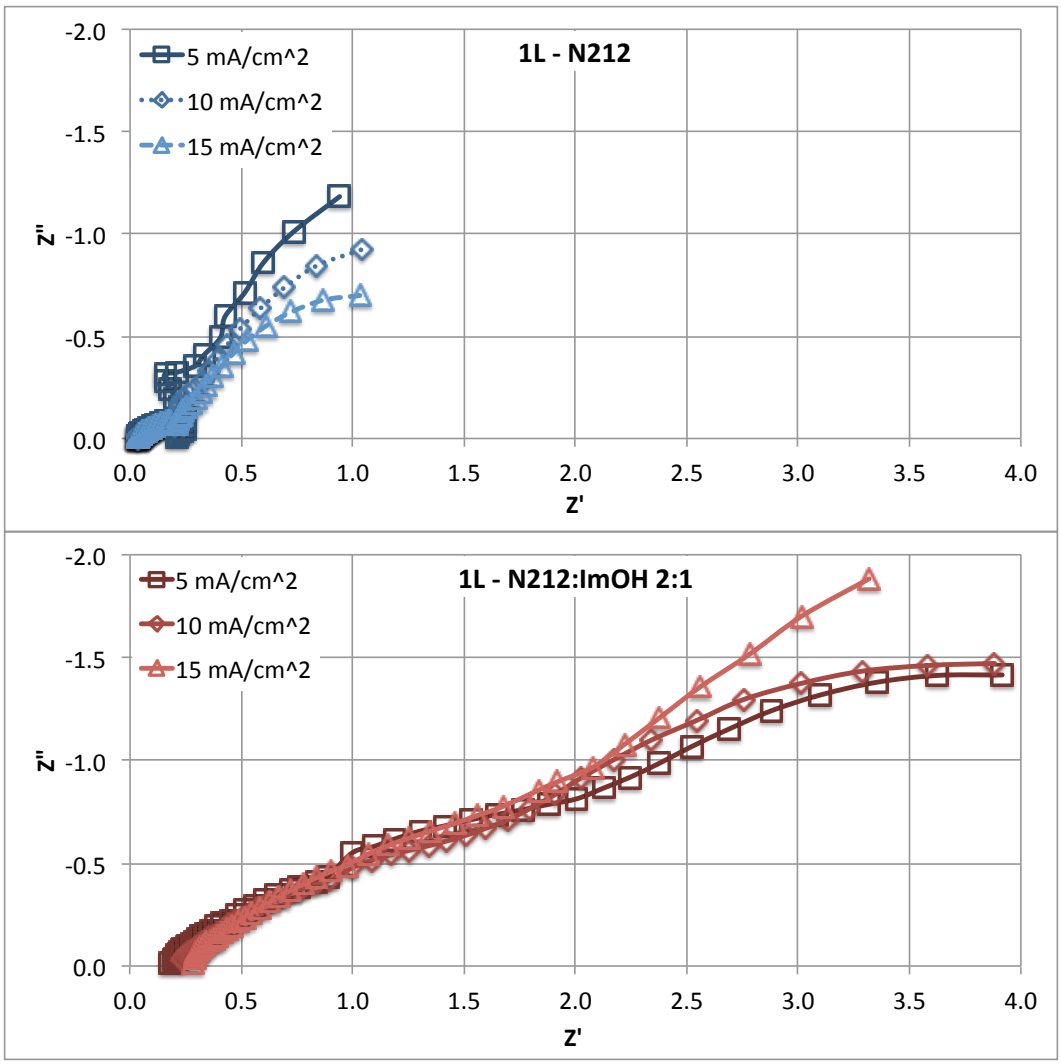

Figure 4.7 Nyquist plots of N212 (top) and N212:ImOH 2:1 (bottom) DMFCs operated at 60°C with selected current densities plotted on the same scale.

Table 4.1: High frequency resistance and charge transfer resistances for DMFCs operating at 60°C with unmodified N212 and N212:ImOH 2:1 MEAs.

N212				
Current Density	R_{HF} (Ω)	% Error	R_{ct} (Ω)	% Error
5 mA/cm^2	0.0196	2.83	0.469	4.49
10 mA/cm^2	0.0232	2.98	0.378	5.69
15 mA/cm^2	0.0233	1.41	0.416	2.41
N212:ImOH 2:1				
Current Density	R_{HF} (Ω)	% Error	R_{ct} (Ω)	% Error
5 mA/cm^2	0.0362	1.26	2.50	5.00
10 mA/cm^2	0.0345	3.18	2.79	3.72
15 mA/cm^2	0.0354	2.25	4.03	4.80

4.2.4 Multi-layered MEAs

Due to the negative effects of having platinum-imidazole interactions at the catalyst layer-membrane interface, it is desirable to keep the imidazole groups isolated to the bulk membrane in the MEA. However, since polymer chains in the membrane undergo constant segmental motion during cell operation, keeping them in one place is a significant challenge. Additionally, attaching the electrodes using hot pressing relies on polymer segments from the membrane moving into the catalyst layer in order to make a good CL-membrane connection.

Here we attempt to isolate the imidazole groups of the modified membrane from the CL through the use of a physical barrier. We do this by creating a 3-layer (3L) membrane, using the procedure described in Section 6.3.3, with a single layer of N212:ImOH 2:1 between two layers of unmodified N212. When this 3-layer membrane is hot pressed into an MEA, the CL-membrane interface should not suffer from platinum-imidazole interactions. For comparison, 3-layers of unmodified N212 were also constructed into a multilayer membrane and assembled into an MEA.

The 3L MEAs were assembled into fuel cell hardware and MEA impedance was measured during fuel cell operation in order to observe the effects of using unmodified N212 as a barrier between the ImOH modified membranes and the platinum catalyst. The resulting EIS spectra are shown in Figure 4.8. From Figure 4.8a and 4.8c, we see that there is little change in charge transfer resistance when using 3 layers of unmodified N212 as compared with the single layer. There is an increase in the high-frequency resistance due to the increase in membrane thickness.

When we compare Figure 4.8b and 4.8d, we see that layering the ImOH modified membrane between two unmodified layers of N212 results in a dramatic decrease in

charge transfer resistance, as evidenced by the significant decrease in the high frequency semicircle of Figure 4.8d. Additionally, the 3L-N212:ImOH 2:1 MEA was able to maintain stabile operation at higher current densities than the single layer MEA, allowing for impedance measurements to be made up to 50 mA/cm^2. In the 3L-N212:ImOH 2:1 MEA, the charge transfer resistance decreases as cell current density increases, resulting in R_{ct} values that approach those of the N212 MEAs. A summary of high frequency and charge transfer resistances for each cell is provided in Table 4.2 and 4.3.

The 3L MEAs also showed improved fuel cell performance, and stability, during polarization curve measurements. First cycle polarization curves for one and three layer MEAs are shown in Figure 4.9. It is clear that there is an improvement in performance simply from using a thicker membrane, which inherently reduces fuel crossover and will be discussed further in the following section. Looking at the activation loss region below 20 mA/cm^2, we see that using three layers of unmodified N212 has little effect on the drop in cell voltage in this region with the 3L-N212 MEA loosing 0.11V and the 1L-N212 MEA loosing 0.12V due to activation losses. However, layering the N212:ImOH 2:1membrane results in a decrease in activation loss from 0.26V with the 1L MEA to 0.17V with the 3L MEA. This reduction in activation loss, along with the reduction in charge transfer resistance, suggests that layering the modified membrane between unmodified layers does reduce unwanted interactions between the imidazole and catalyst layers.

Above 20 mA/cm^2, the 3L-MEAs show improved performance with increased peak power density and max current density. Layering the unmodified N212 resulted in a 60% increase in current density at 0.1V from 200 mA/cm^2 to 320 mA/cm^2, while layering the N212:ImOH 2:1 membrane increased 40% from 100 mA/cm^2 to 140 mA/cm^2. Peak power density improved 84% for the 3L-N212 MEA from 30 mW/cm^2 to 55 mW/cm^2, and 54% for the 3L-N212:ImOH 2:1 MEA from 12 mW/cm^2 to 19 mW/cm^2. Additionally, the 3L-MEAs showed better stability for the duration of testing.

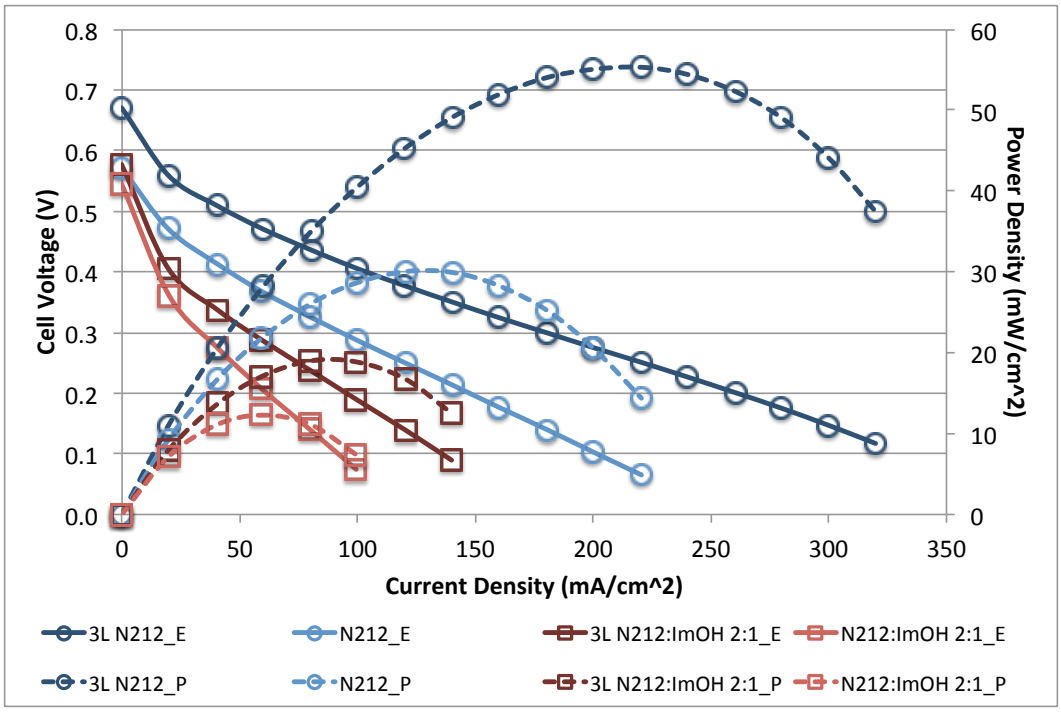

Figure 4.9: First cycle polarization curves for DMFCs operating at 60°C with 1L and 3L MEAs constructed from unmodified N212 and N212:ImOH 2:1.

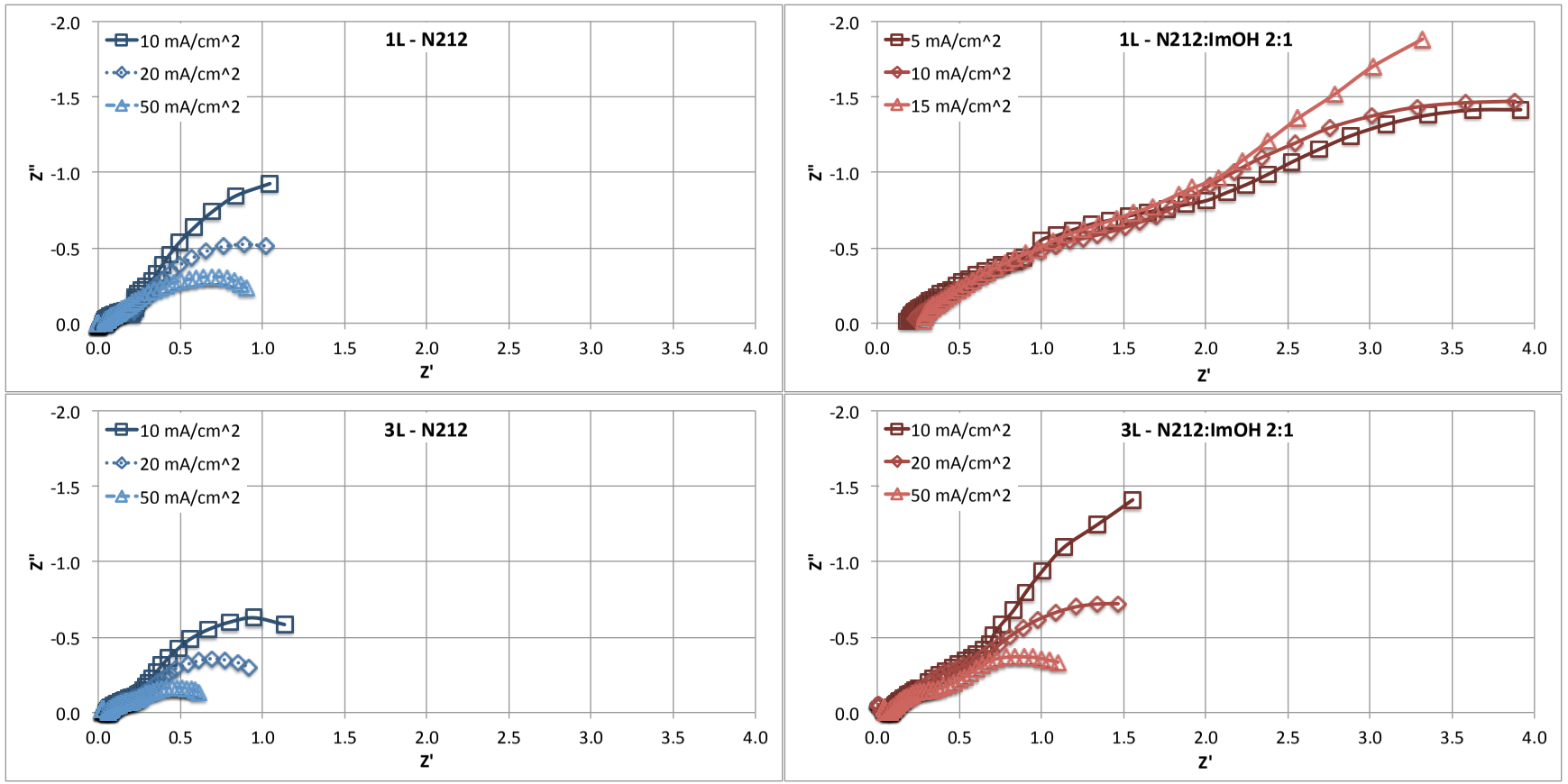

Figure 4.8: Nyquist plots of EIS spectra at select current densities for DMFCs operated at 60°C using MEAs constructed of N212 (a), 3L N212 (b), N212:ImOH 2:1 (c), and 3L N212:ImOH 2:1 (d).

Table 4.2: Summary of R_{HF} and R_{ct} values for 1L- and 3L-N212 MEAs operated in a DMFC at 60°C under various current densities.

1L-N212				
Current Density	R_{HF} (Ω)	% Error	R_{ct} (Ω)	% Error
5 mA/cm^2	0.0196	2.83	0.469	4.49
10 mA/cm^2	0.0232	2.98	0.378	5.69
15 mA/cm^2	0.0233	1.41	0.416	2.41
20 mA/cm^2	0.0265	1.94	0.342	3.75
30 mA/cm^2	0.0279	2.46	0.202	4.48
40 mA/cm^2	0.0267	2.77	0.553	12.6
50 mA/cm^2	0.0270	2.53	0.699	16.1
3L-N212				
Current Density	R_{HF} (Ω)	% Error	R_{ct} (Ω)	% Error
5 mA/cm^2	0.0473	1.73	0.349	7.95
10 mA/cm^2	0.0491	1.06	0.332	5.43
15 mA/cm^2	0.0483	1.90	0.369	8.11
20 mA/cm^2	0.0492	1.60	0.386	7.43
30 mA/cm^2	0.0554	1.46	0.206	3.31
40 mA/cm^2	0.0537	0.858	0.315	2.52
50 mA/cm^2	0.0552	1.04	0.302	3.10

Table 4.3: Summary of R_{HF} and R_{ct} values for 1L- and 3L-N212:ImOH 2:1 MEAs operated in a DMFC at 60°C under various current densities.

1L-N212:ImOH 2:1				
Current Density	R_{HF} (Ω)	% Error	R_{ct} (Ω)	% Error
5 mA/cm^2	0.1539	1.35	2.50	5.00
10 mA/cm^2	0.189	0.718	2.79	3.72
15 mA/cm^2	0.222	1.15	4.03	4.80
20 mA/cm^2	———	———	———	———
30 mA/cm^2	———	———	———	———
40 mA/cm^2	———	———	———	———
50 mA/cm^2	———	———	———	———
3L-N212:ImOH 2:1				
Current Density	R_{HF} (Ω)	% Error	R_{ct} (Ω)	% Error
5 mA/cm^2	0.0630	1.66	2.26	33.0
10 mA/cm^2	0.0604	0.977	2.75	22.2
15 mA/cm^2	0.0610	0.660	2.38	11.7
20 mA/cm^2	0.0623	0.632	2.11	11.3
30 mA/cm^2	0.0521	1.34	0.327	5.63
40 mA/cm^2	0.0667	0.481	0.9722	4.05
50 mA/cm^2	0.0701	0.550	0.801	3.89

4.2.5 Membrane Selectivity

Membrane selectivity can be characterized by measuring fuel crossover through the membrane, while assembled in fuel cell testing hardware. The technique for measuring fuel crossover used in this study was developed by Xiaoming Ren *et. al.*[21, 22] and involves the complete electro-oxidation of crossed-over methanol at the cathode in an inert atmosphere.

After fuel cell testing, the cathode oxygen feed was switched to nitrogen and methanol crossover was measured in the fuel cell hardware using the procedure described in Section 6.3.4. The cell setup for crossover measurements is shown in Figure 4.10. Linear sweep voltammetry (LSV) is used to apply voltage to the cell, and methanol is electro-oxidized at the cathode producing current. At sufficiently high voltages, a limiting current is reached. This current is limited by the amount of methanol permeating the membrane to the cathode. Improvement to the membrane selectivity would have the effect of reducing this limiting current.

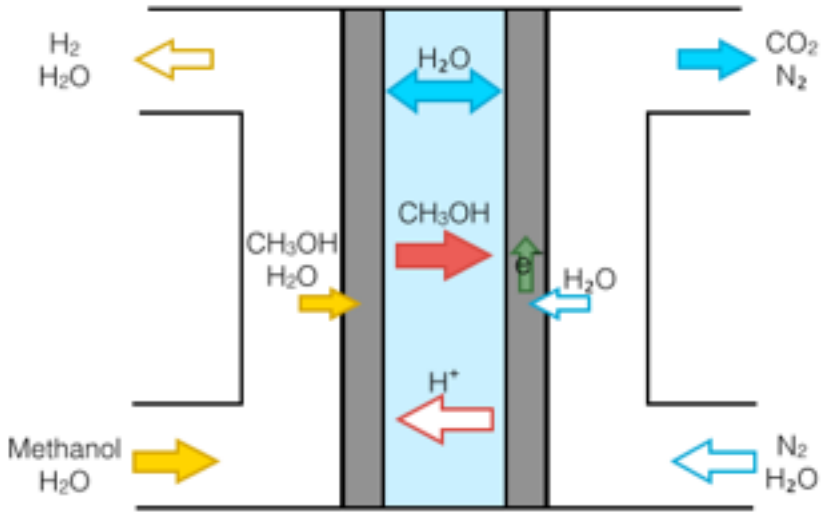

Figure 4.10: Diagram of cell setup for crossover measurements. Cathode feed is switched from oxygen to nitrogen.

Crossover measurements performed on the 1L- and 3L-N212 membranes are shown in Figure 4.11. Both membranes show the characteristic plateau indicating the limiting current due to methanol crossover. The 1L-N212 produces a limiting current of ~115 mA/cm^2, while the 3L-N212 membrane has a limiting current of just 55 mA/cm^2. The lower crossover of the 3L-N212 membrane is a result of the increased membrane thickness.

The crossover measurements for the 1L- and 3L-N212:ImOH 2:1 membranes are also shown in Figure 4.11. The limiting current for the N212:ImOH 2:1 membranes decreased from 62 mA/cm^2 for the 1L membrane to 22 mA/cm^2 for the 3L membrane. As with the unmodified membranes, increasing the thickness from a single layer to 3 layers results in the decrease in limiting current observed here.

Comparing the crossover current of the modified and unmodified membranes, we see that the addition of ImOH to N212 does reduce crossover current. For the single layer membranes, the presence of imidazole decreases crossover current by about 46% from 115 to 62 mA/cm^2. In the 3L membranes, the reduction in crossover current is about 60%, from 55 to 22 mA/cm^2. From these measurements, it is clear that by incorporating imidazole into the membrane structure it is possible to reduce methanol crossover, increasing membrane selectivity.

In addition to the decrease in crossover current, it is also observed that the N212:ImOH 2:1 membranes do not result in a well defined plateau. This is particularly evident in the 3L membrane. Instead of reaching a plateau, the ImOH modified membranes exhibit a slope change followed by a continued, linear increase in current. This behavior is indicative of an internal short circuit[62]. Typically, this sort of internal short circuit is the result of pin holes in the membrane. However, in the ImOH modified membranes, this behavior is likely caused by inhomogeneities in the distribution of the ImOH, resulting in some regions of the membrane that contain no imidazole, allowing higher methanol crossover through these regions. These unmodified regions are effectively ‘holes’ in the ImOH membrane.

While in-situ crossover measurements provide a good indicator of membrane selectivity, it is desirable to observe the effects of the imidazole through more direct measurement of methanol diffusion through the membrane. Pulse field gradient spin-echo NMR measurements were performed on the single layer N212 and N212:ImOH 2:1 membranes by graduate student Matt Dodd. Figure 4.12 shows the measured diffusion coefficients of methanol in the membranes at various temperatures. It is clear that the addition of ImOH to the membrane decreases methanol diffusion at all temperatures measured, thus reducing the ability of methanol to permeate the membrane during fuel cell operation. This is in good agreement with the observations made from measuring crossover current using LSV.

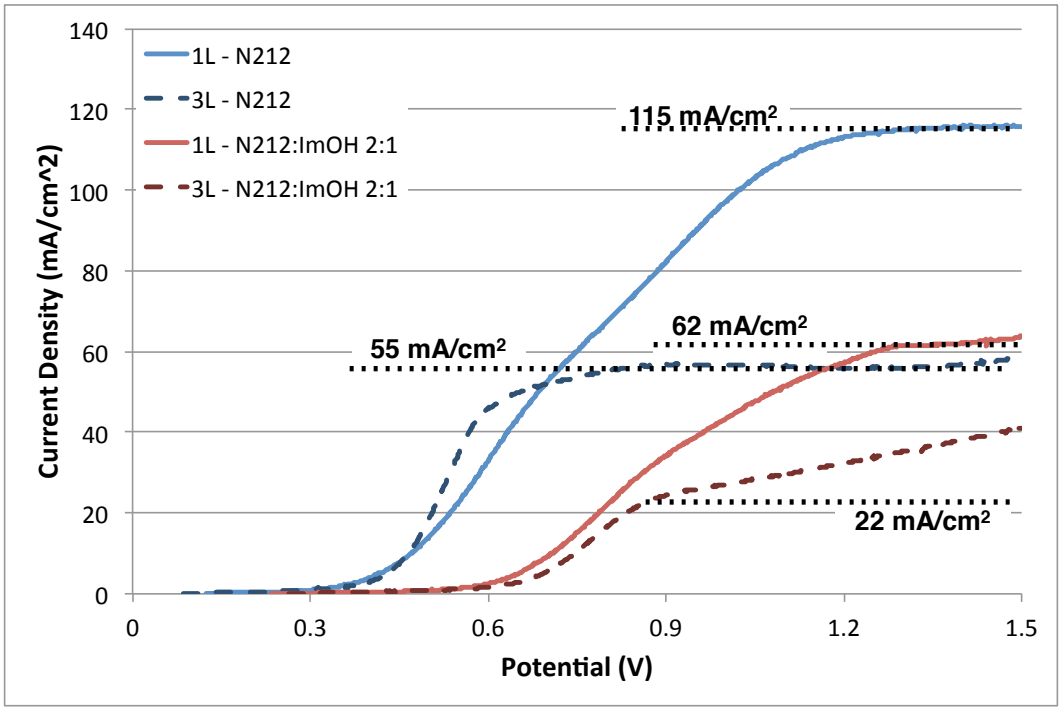

Figure 4.11: Methanol crossover current as determined by LSV of 1L- and 3L-N212 and N212:ImOH 2:1 membranes at 60°C.

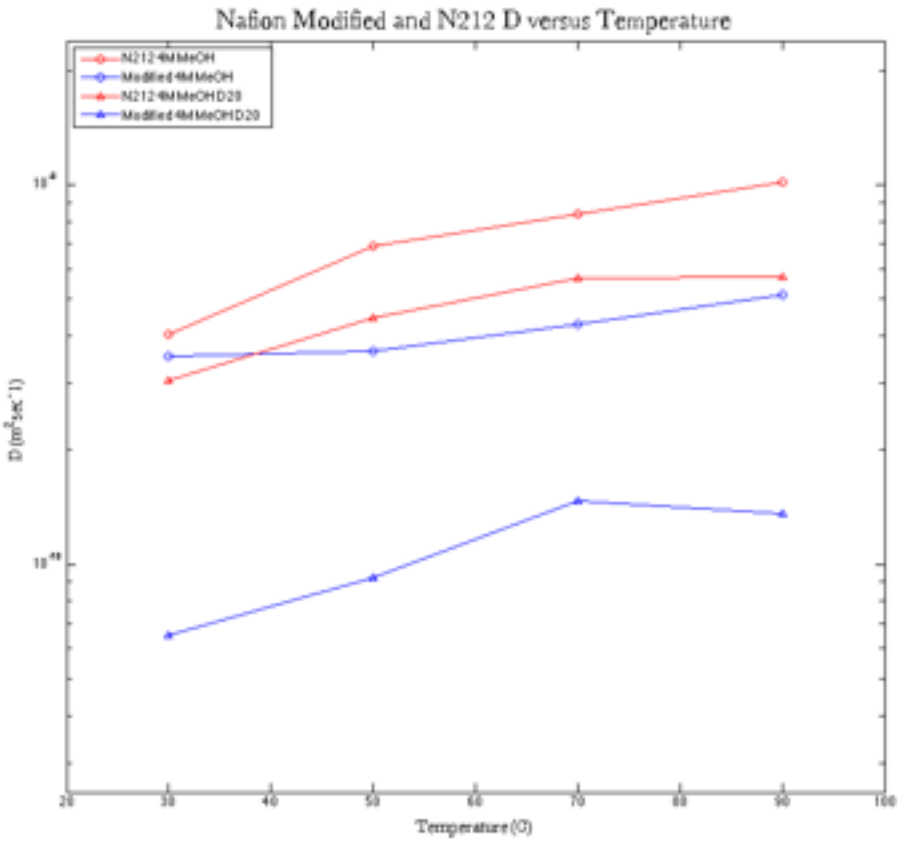

Figure 4.12: Methanol diffusion coefficients at select temperatures as determined by pulse field gradient spin-echo NMR.

4.3 Conclusions

MEAs were constructed using N212 and N212:ImOH 2:1 membranes and tested in DMFCs operating at 60°C. Modification of N212 with ImOH resulted in reduced fuel cell performance and stability. Fuel cell polarization of the N212:ImOH 2:1 MEA showed a greater reduction in cell voltage due to activation loss. From MEA impedance measurements, it was determined that the imidazole containing membranes significantly increase the charge transfer resistance in the electrodes, likely resulting from unwanted interactions between the nitrogens of the imidazole and the platinum catalyst[60, 61].

In order to prevent imidazole-platinum interaction, multilayered membranes were constructed by hot pressing the N212:ImOH 2:1 membranes between two unmodified N212 membranes. MEAs made from these multilayered membranes showed improved performance and stability during fuel cell testing, and as well as a smaller drop in cell voltage from activation loss. Impedance measurements showed that layering the ImOH membrane resulted in a significant decrease in charge transfer resistance, as compared with the single layer MEA. These improvements in cell performance, resulting from the use of multilayered membranes, demonstrate that it is possible to control the interactions between the different components of the fuel cell.

Methanol crossover measurements using LSV showed a significant reduction in crossover current cells using the N212:ImOH 2:1 MEAs. This reduction in crossover current suggests that the presence of imidazole in the membrane inhibits the movement of methanol across the membrane. Diffusion coefficients of methanol in the membranes as determined by PFG NMR showed that the diffusion of methanol in the ImOH membrane is reduced, confirming observations made from LSV crossover experiments.

Chapter 5

Summary

In this work the properties of Nafion® 212 (N212) membranes modified with 4(5)-hydroxymethyl imidazole (ImOH) were investigated. Chapter 2 examined the structure and thermal properties of these ImOH modified membranes. NMR studies showed that the nature of the bond between the ImOH and the SO_3^- end groups of the polymer side chains is dependent on the concentration of ImOH within the membrane. Using an SO_3^-:ImOH ratio of 1:1 results in the formation of a salt between the nitrogen of the ImOH ring and the SO_3^- end groups. Changing the ratio to a 2:1 mix allows for the formation of ester bonds between the ImOH and the SO_3^- end groups. Since the attachment of the imidazole to the polymer structure through a covalent bond is desired, the 2:1 membranes are of highest interest.

DMA studies revealed that the presence of ImOH in the membrane has very complex effects on the polymer structure. The observed increase in *α*- and *β*- relaxation temperatures, as well as broadening and decreased intensity of the *α*- relaxation tan(δ), are consistent with cross-linking behavior. This suggests that the ImOH may be acting as a crosslink between side chains. At the same time, an increase in the *γ*- relaxation temperature and tan(δ) peak intensity indicates plasticization of the PTFE backbone structure by the ImOH. Despite the slight plasticization of the backbone, the addition of ImOH to the polymer structure reduced the amount of sample elongation during testing, allowing for testing to continue to higher temperature. This is consistent with the increased thermal stability seen in the TGA experiments.

In Chapter 3, the effects of ImOH on membrane water up-take and swelling were examined, along with proton conductivity. DVS measurements showed that the addition of ImOH results in both a reduction in the total water up-take of the membranes, as well as a reduction in the rate at which water is sorbed and desorbed. The reduction in membrane water content at a given RH was also seen in the TGA loss stage below 250°C, where it was seen that increasing membrane ImOH content reduced the mass loss due to water. This result is in good agreement with the decrease in measured λ values with increased ImOH content.

SAXS studies showed that the ImOH membrane exhibits less swelling of the ionic domains at a given RH than the unmodified Nafion® membrane. It was expected that less water up-take would result in less swelling of the membrane. However, the N212:ImOH 2:1 membrane also showed less swelling for a given water content (λ). This suggests that the water in the modified membranes is not as confined to the ionic domains as in the unmodified N212.

The reduced swelling of the modified membrane ionic domains is likely a result of both the reduced water up-take of the membrane, as well as the stiffening of the side chains due to the cross-linking effect of ImOH, as seen by DMA, that prevents the ionic domains from expanding to accommodate additional water. Additionally, the ImOH was seen to plasticize the polymer backbone. Plasticization of the backbone matrix by the ImOH is supported by the broadening and decrease in intensity of the matrix knee in the SAXS scattering profile. This plasticization could allow for sorbed water to penetrate the backbone matrix. With water no longer being localized to the ionic domains, the modified membrane would exhibit less ionic domain swelling for a given λ, as was observed in the SAXS measurements.

Ionic conductivity measurements showed that the addition of ImOH decreases the magnitude of conductivity at all RH, and for a given λ, at 50°C. The dependence of

conductivity on RH in the modified membranes remains the same as that of the unmodified N212. Looking at the temperature dependence of conductivity, it was seen that all membranes exhibit Arrhenius type behavior, allowing for the calculation of the proton conducting activation energy. Interestingly, the activation energy for proton conduction (E_a) of N212 and N212:ImOH 2:1 at 95% RH is equal. Having the same E_a means that protons are able to move through the N212:ImOH 2:1 membrane as freely as in the N212 membrane, despite the N212:ImOH 2:1 membrane having lower water content than the N212.

The lower magnitude of conductivity in the N212:ImOH 2:1 membrane is a result of having fewer charge carrier present in the membrane due to the ImOH covalently attaching through the SO_3^- end groups. The 2:1 ratio has cut the number of available protons in half, reducing the magnitude of conductivity. The ability of the modified membranes to allow for the conduction of protons with the same E_a as N212, while containing less water, strongly suggests that the imidazole is acting as a proton solvent, compensating for the reduction in water content. The important thing to note here is that the energy barrier to proton conduction in both the N212 and N212:ImOH 2:1 membranes at 95% RH is the same, despite the difference in the magnitude of conductivity.

At this point, the properties of N212 membranes modified with ImOH have been studied outside of the fuel cell environment. It has been seen that the incorporation of ImOH into the polymer structure results in improved thermal stability, while plasticizing the backbone matrix. This plasticization allows for sorbed water to penetrate the PTFE matrix, resulting in less swelling of the ionic domains. When fully hydrated, the modified membranes now have narrower ionic channels, and contain less water per acid group. Despite this, the activation energy for proton conduction at 95% RH of the N212:ImOH 2:1 membrane is the same as that of the unmodified N212. This effect is a result of the imidazole assisting water in proton solvation, and the alignment of the imidazole groups from confinement within the narrowed ionic channels.

Modification of N212 with ImOH in an effort to replace water with an immobilized proton solvent has shown promising results outside of the fuel cell environment. Chapter 4 investigated the effect of ImOH modification on the performance of direct methanol fuel cells. Initial testing showed relatively poor performance and cell stability. In-situ MEA impedance measurements revealed that MEAs made with the ImOH modified membranes had significantly higher charge transfer resistance than the unmodified MEAs. It is thought that this rise in charge transfer resistance is a result of the formation of complexes between the imidazole in the membrane and the platinum catalyst, reducing catalytic activity.

In an effort to isolate the imidazole from the platinum catalyst, the modified membranes were layered between two unmodified membranes and hot pressed to form multi-layered MEAs. These MEAs showed significantly improved performance and cell stability. Impedance measurements also showed significant reduction in charge transfer resistance as compared to the single layer membrane. The R_{ct} of the multi-layer MEA is similar to that of the unmodified MEA, showing that layering the membranes did provide a barrier to prevent undesired imidazole-platinum interactions.

Imidazole was initially chosen as a proton solvent because of its similar chemical nature to water. Immobilization of the imidazole in the polymer structure was desired in

order to reduce fuel crossover by removing the primary mode of transportation of fuel through the membrane: electro-osmotic drag of the fuel through the water channels. Ex-situ study of the modified membrane properties has shown that the immobilization of imidazole in the membrane reduces both membrane water content and ionic domain size. Additionally, the rate of water sorption/desorption was decreased, indicating that the imidazole slows the movement of water within the membrane. This behavior is likely related to the cross-linking effect of the imidazole, which reduces the motion of the SO_3^- end groups. Considering these effects, it was expected that the ImOH modified membranes would have lower fuel crossover as compared to the unmodified membranes.

Methanol crossover was studied by the electro-oxidation of crossed over methanol at the cathode in an inert atmosphere. The crossover rate was characterized by the limiting current, which is limited by the flow of methanol from the anode to cathode through the membrane. Crossover measurements showed that modification of the membranes reduced methanol crossover by 50-60%.

Diffusion coefficients of water and methanol in the membranes were measured using PFG-NMR. These measurements confirmed observations made from the crossover current, wherein the diffusion of both methanol and water through the ImOH modified membranes was reduced. Additionally, this reduction in water diffusion coefficient is in good agreement with the slower water sorption/desorption kinetics seen from DVS experiments.

Considering all these factors, it appears that imidazole can be immobilized into a polymer structure while retaining its proton solvating capabilities, and replacing water for proton transport. This was demonstrated in Chapter 3. The use of an immobilized proton solvent also reduced fuel crossover by inhibiting the movement of methanol and water through the membrane, as demonstrated in Chapter 4. This system of Nafion® and ImOH was investigated as a proof-of-concept system, and sets the stage for further development of immobilized proton solvent systems using novel polymer membranes.

Chapter 6

Experimental Procedures and Methods

This chapter describes the experimental methods and procedures used to obtain all previously discussed results. This experimental chapter is divided into sections corresponding with the appropriate chapters in which the methods and procedures were used.

6.1 Chapter 2

6.1.1 Membrane Modification

Commercial Nafion® 212 (N212), with a dry thickness of 2 mil (50 µm) and equivalent weight (EW) of 1100 g/mol, was obtained from Ion Power, Inc and used as-received for the control membrane. 4(5)-hydroxymethyl imidazole (ImOH) was obtain from Sigma Aldrich and was used as-received. Samples of N212 were weighed in air and the mass used to calculate the amount of ImOH needed to be added to obtain membranes with an acid:base ratio of 1:1 and 2:1. In this case, a 2:1 ratio indicates that there are two sulfonic acid groups for each ImOH inside the membrane.

100 mL solutions of ImOH in water were made, and membranes were left to soak in the solution, with stirring, for 24 hours. After soaking, the membranes were laid flat and left to air dry over night prior to testing.

6.1.2 Thermogravimetric Analysis

Thermal stability of the ImOH modified membranes was measured using Thermogravimetric Analysis (TGA). Measurements were performed in a nitrogen atmosphere heating from 50°C to 550°C at a rate of 20°C/min.

6.1.3 Differential Scanning Calorimetry

Thermal transitions were studied under nitrogen using differential scanning calorimetry (DSC). Membrane samples of approximately 5 mg were loaded into aluminum sample pans. DSC measurements were performed on a Perkin Elmer DSC 8000 under a nitrogen atmosphere. Samples were heated from -100°C to 200°C at a rate of 10°C/min, held at 200°C for 10 min, cooled to -100°C at 10°C/min, held at -100°C for 10 min, and heated to 200°C at a rate of 10°C/min. Thermal transition temperatures from the second heating were reported for results.

6.1.4 Dynamic Mechanical Analysis

Mechanical properties were measured under nitrogen flow using a Triton Technologies Tritec 2000 DMA in the tension geometry. Samples were cut to a rectangular geometry with 1 cm width and long enough to be mounted appropriately (approximately 2.5 cm in length). Sample length was measured after mounting. The sample was cycled at 0.1, 1.0, and 10.0Hz with a tension displacement of 0.1% of the sample thickness.

Temperature scan experiments were conducted in the temperature range of -150°C to 250°C, and heating at a rate of 2°C/min.

6.2 Chapter 3

6.2.1 Dynamic Vapor Sorption

Water uptake measurements were performed on the polymer membranes using a DVS-Advantage from Surface Measurement Systems. Dynamic Vapor Sorption (DVS) measures membrane water uptake gravimetrically using a microbalance, with mass resolution of ±0.1 µg, as sample chamber humidity is stepped under isothermal conditions. Membrane samples of 5 to 10 mg were loaded into the stainless steal mesh sample pan (400 holes/in) to allow the vapor to flow directly to all surfaces of the sample.

The sample chamber and water dew point were held at a constant temperature while the relative humidity (RH) of the sample chamber is controlled by mixing wet and dry nitrogen gas feeds. The total flow through the sample chamber is 200 sccm.

Dry sample weight was determined by holding the sample at temperature and 0%RH for 2 hours, after which, the initial dry sample weight, M_0, was set. After drying, relative humidity was stepped from 0% to 90%RH in 10% steps, then to 95% and 98% before returning to 0% along the same steps. Each humidity step was held for 6 hours or until the change in weight, $\Delta M/M_0$, was less than 0.005 %/min.

The weight of water absorbed by the membrane sample, M_W, is defined by the measured sample weight, M_{mbr}, and the initial dry weight as, $M_W = M_{mbr} - M_0$. For comparison of water uptake between modified membranes, it is desirable to describe the weight of water absorbed in terms of water content, λ. The term λ is defined as the number of water molecules per sulfonic acid group within the membrane[2], and is calculated at the end of each step by

$$\lambda = \frac{y \cdot EW}{x \cdot M_{H_2O}} \qquad [6.1]$$

Where y is the net change in weight percent of the sample, EW is the equivalent weight of the ionomer (1100 *g/mol*), M_{H_2O} is the molar mass of water (18 *g/mol*), and x is the ionomer concentration in the dry membrane (x = 1 for dry N212). The water content at

0%RH is assumed to be zero, though there may be residual bound water that can only be removed through heating.

Water uptake kinetics were investigated using the measured weight change as a function of time, *t*, for each RH step with a method outlined by *Kusoglu et al*.[49, 50] By this method, the inverse time constant, k_s, was determined for each RH step using

$$\frac{M(t)-M_0}{M_\infty-M_0}=\frac{M_W(t)}{M_W^\infty}=1-\exp(-k_s t)=1-\exp\left(-\frac{t}{\tau}\right) \qquad [6.2]$$

where τ is the time constant.

6.2.2 Ionic Conductivity

Through plane proton conductivity of the membranes was measured using four-terminal AC impedance spectroscopy. Measurements were performed using a Scibner Associates Inc. Membrane Test System 740 (MTS) and Schlumberger Technologies Inc SI 1260 impedance/gain-phase analyzer. The MTS electrode configuration is shown in Figure 6.1.

Testing procedure consisted of assembling the sample into test cell, conditioning the membrane, and taking impedance measurements throughout the test cycle. The procedure used in this work is based off the procedure outlined by Kevin Cooper[51], and is described in detail below.

Sample/cell assembly — The membrane sample was cut to a 2.5 X 1.0 *cm* rectangle and the thickness, *L*, measured using a Mitutoyo micrometer at ambient conditions (~22°C, 30%RH). The membrane was placed between gas diffusion layers (GDL) (Ion Power, Inc Sigracet® GDL 10 BC) attached to solid platinum backing electrodes with conductive carbon paint. The assembly was compressed using a calibrated force spring and dial displacement indicator to a compressive load of 2.197 ± 0.017 MPa (319 ± 2.5 psi). The GDL allows water vapor to access the entire membrane surface while sample is under compression.

Test conditions — Isothermal humidity scans and constant RH temperature scans were performed on each membrane. RH was controlled using a mixture of wet and dry nitrogen with total flow rate of 500 sccm.

Isothermal humidity scans were performed at 50°C. Samples were conditioned at 70%RH for 2h followed by stepping RH from 70 to 20 to 90% at 10% increments, then to 95%RH. Each RH step was held for 30 min for equilibration prior to measuring membrane resistance.

Temperature scans at constant RH were performed at 25, 50, and 95%RH. The sample chamber was pressurized to 193 kPa (28 psi) and temperature was stepped from 30 to 120°C in 10°C steps, holding each step for 45 min for equilibration prior to measuring membrane resistance.

Impedance measurement — After equilibrating at each testing condition, a controlled voltage, frequency sweep impedance spectroscopy measurement was

performed (10 mV_{AC} at 0 V_{DC}, 2 MHz - 1 Hz, 10 steps/decade). Membrane resistance is given by the high frequency intercept and was determined by fitting the impedance spectra with an equivalent circuit model. The through-plane proton conductivity (σ in *S/cm*) is determined by

$$\sigma = \frac{L}{RA} \qquad [6.3]$$

Where R is the high frequency membrane resistance in *Ω*, *L* is the membrane thickness in *cm*, and *A* is the cross-sectional area (0.5 cm^2).

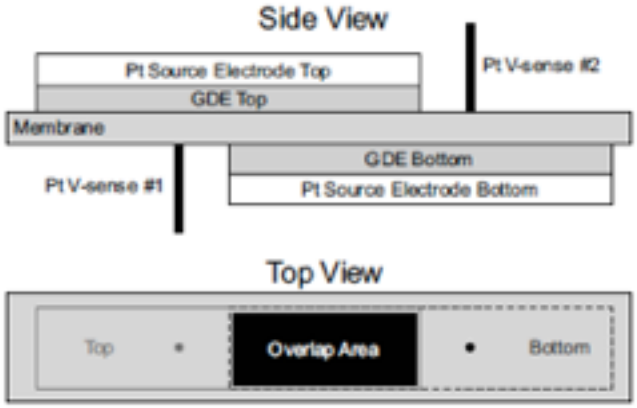

Figure 6.1: Illustration of the electrode/sample configuration used by the Scribner MTS 740[51].

6.2.3 Small Angle X-ray Scattering

Membrane morphology and was studied using Small Angle X-ray Scattering (SAXS). Measurements were performed with the SAXS instrument at the Advanced Light Source (ALS) at Lawrence Berkeley National Laboratory using beam line ALS 7.3.3.

Humidity measurements were performed at 50°C using a humidity stage developed, and described by Jackson *et. al.*[64] Humidity steps used were 30, 50, 75, 85, 90, and 95% RH and each step was held for 1 hour. At each humidity, scattering curves were collected every 2 minutes for 1 hour. The sample was exposed to the beam for 45 seconds with 75 seconds between scans. The beam was moved to a new area of the sample between each humidity step.

6.3 Chapter 4

6.3.1 Membrane Electrode Assembly

Gas diffusion electrodes (GDE) for direct methanol fuel cells (DMFC) were obtained from IRD Fuel Cells LLC. GDEs were constructed of carbon paper gas diffusion layer and catalyst layer containing catalyst loadings of 2.0 mg/cm^2 PtRu/C for the anode, and 1.5 mg/cm^2 Pt/C for the cathode. N212 and N212:ImOH 2:1 membranes were used as described in Section 6.1.1. The membrane electrode assembly (MEA) was constructed by hot pressing using a hydraulic hot press from Carver, Inc. Membranes were cut to 7.5 cm squares and sandwiched between an anode and cathode GDE cut to 2 cm X 2.5 cm, giving 5cm^2 active area. This MEA assembly was then hot pressed at 30°C above the glass transition temperature of the membrane (145°C for N212, 180°C for N212:ImOH 2:1), as determined by DMA (Section 2.2.3), with 500 lbs of pressure (approximately 650 psi) for 4 minutes. After removing from the hot press, the MEA was allowed to cool to room temperature prior to assembling into fuel cell hardware.

6.3.2 Fuel Cell Testing and MEA Impedance

For fuel cell testing, the MEAs are assembled into single cell fuel cell hardware with serpentine flow fields from Fuel Cell Technologies Inc, and liquid fuel line attachments for the anode. Liquid fuel was delivered to the cell using a Minipuls 3 peristaltic pump from Gilson, Inc. The fuel cell hardware is connected to a fuel cell test stand from Scribner Associates, Inc.

The fuel cell was heated to 60°C with a fully humidified nitrogen feed through the cathode for 2-3 hours, and anode open to air, to allow for membrane hydration. The cathode was then switched to a fully humidified oxygen supply flowing at 28 mL/min at 60°C with a back pressure of 15 psig. The anode was switched to liquid fuel flowing at 25 mL/min. The liquid line was not heated or given back pressure. Liquid fuel used was 1M methanol in water.

Cell testing began shortly after applying fuel as the cell open circuit voltage (OCV) stabilized (approximately 5 minutes). The cell was then cycled between OCV and half OCV at 3 minute intervals for 30 minutes. After OCV cycling, OCV was held for 15 minutes, then a polarization curve was obtained by stepping current in 20 mA/cm^2 steps, holding each step for 60 seconds, then reversing the scan when the cell potential dropped below 0.12 V. This was followed by a series of constant current steps and AC impedance measurements. Constant current was held for 15 minutes at 5, 10, 15, 20, 30, 40, and 50 mA/cm^2, after which AC impedance was measured at each current density over the frequency range 1 to 100,000 Hz. After all current steps and impedance measurements were completed, the cell was left at OCV for 15 minutes followed by three polarization curves performed in the same manner described above. After cycling, the cell was again set to OCV for 15 minutes.

Impedance spectra were fitted using equivalent circuit modeling to determine the ohmic resistance of the MEA, and charge transfer resistances associated with the electrodes.

6.3.3 Multi-layered MEAs

Multi-layered membranes were constructed by hot pressing 3 membranes together prior to constructing the MEA. Two types of multi-layered membranes were made. The first consists of 3 layers of N212 for use as a control. The second is made up of an N212:ImOH 2:1 membrane sandwiched between two N212 membranes. The membranes were hot pressed at 145°C for 10 minutes under 500 lbs of pressure to ensure good adhesion between the layers. After layering, the multi-layer membranes were then made into MEAs using the procedure in Section 6.3.1 (at 145°C). A diagram of the layering process is shown in Figure 6.2.

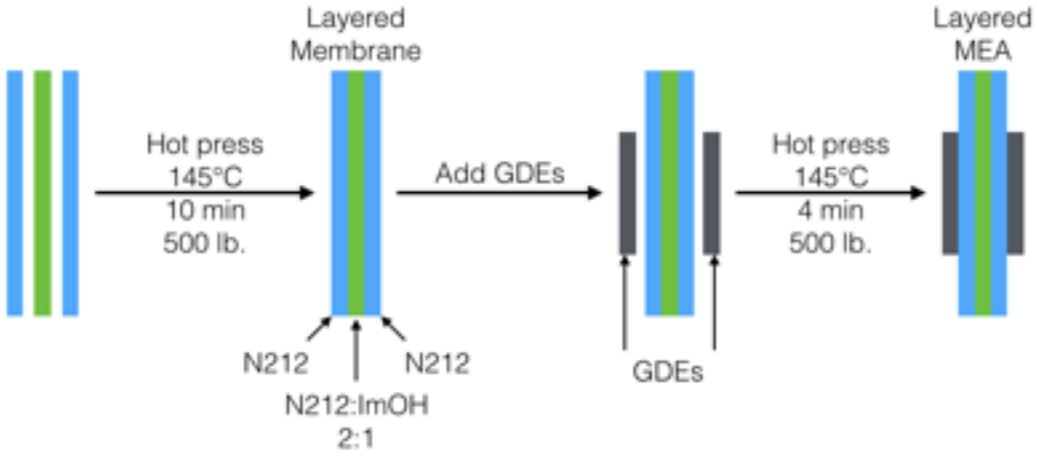

Figure 6.2: Diagram of assembly and structure of the multi-layered membrane electrode assembly.

6.3.4 Fuel Crossover Measurements

After fuel cell testing, using the method described in the previous section, the cathode gas feed was switched from oxygen to fully humidified nitrogen with the same flow rate and back pressure. The anode fuel feed remains the same. The cathode side of the cell was purged with nitrogen until the cell voltage dropped to 0.1 V.

When a cell voltage of 0.1 V was reached, the voltage and current connections to the fuel cell hardware were disconnected in order to isolate the cell hardware from the fuel cell test stand. The cell was then hooked up to a Solartron SI 1286 electrochemical interface (Schlumberger Technologies, Inc.) with the reference 1 and counter electrode

leads attached to the anode side of the cell, and the reference 2 and working electrode leads attached to the cathode side. The Solartron system was controlled using Corrware software from Scribner Associates, Inc.

Using an electro-oxidation technique described by Xiaoming Ren *et al.*[21, 22] linear sweep voltammetry (LSV) was used to measure fuel crossover through the membrane. A potentiodynamic experiment was set up in the Corrware software to scan voltage from OCV to 1.5 V at 2 mV/s to obtain a limiting current resulting from the crossover of methanol to the cathode.

References

[1] A. Kusoglu, A. Webber, (2012) Water Transport and Sorption in Nafion® Membrane, in Polymers for Energy Storage and Delivery: Polyelectrolytes for Batteries and Fuel Cells. (eds K.A. Page, C.L. Soles, and J. Runt), American Chemical Society, Washington, DC. doi: 10.1021/bk-2012-1096.ch11.

[2] T.E. Springer, T.A. Zawadzinski, S. Gottesfeld, *J. Electrochem. Soc.*, **138** (1991) 2334-2342.

[3] A.Z. Weber, J. Newman, *J. Chem. Rev.,* **104** (2004) 4679-4726.

[4] T.A. Zawodzinski, C. Derouin, S. Radzinski, R.J. Sherman, V.T. Smith, T.E. Springer, S. Gottesfeld, *J. Electrochem. Soc.,* **140** (1993) 1041-1047.

[5] W.Y. Hsu, T.D. Gierke, *J. Membr. Sci.*, **13** (1983) 307-326.

[6] N. Agmon, *Chemical Physics Letters*, **244** (1995) 456-462.

[7] K.D. Kreuer, S.J. Paddison, E. Spohr, M. Schuster, *Chemical Reviews,* **104** (2004) 4637-4678

[8] P.G. Khalatur, S.K. Talitskikh, A.R. Khokhlov, *Macromol. Theory Simul.*, **11** (2002) 566-586.

[9] K.D. Kreuer, *J. Membr. Sci.*, **185** (2001) 29-39.

[10] S.J. Paddison, *Annu. Rev. Mater. Res.*, **33** (2003) 289-319.

[11] M. Eikerling, A.A. Kornyshev, A.M. Kuznetsov, J. Ulstrup, S. Walbran, *J. Phys. Chem. B*, **105** (2001) 3646-3662.

[12] K.D. Kreuer, *Solid State Ionics*, **94** (1997) 55-62.

[13] M.A. Yandrasits, S.J. Hamrock, In: *Fuel Cell Chemistry and Operation*, A.Herring, et.al., ACS Symposium Series; American Chemical Society: Washington, DC, (2010).

[14] K.M. McGrath, G.K.S. Prakash, G.A. Olah, *J. Ind. Eng. Chem.*, **10** (2004) 1063-1080.

[15] H.W. Cooper, *Chemical Engineering Progress*, **103** (2007) 34.

[16] H. Gasteiger, T. Schmidt, (2013, October). Polymer Electrolyte Fuel Cells. *224th ECS Meeting*. Lecture conducted from Hilton San Francisco, San Francisco, CA.1

[17] W. Vielstich, in: Handbook of Fuel Cells (eds.: W. Vielstich, A. Lamm, H.A. Gasteiger), Wiley (2003): vol. 1, chapter 4, p. 26.

[18] Zhang, J., Zhang, J., In: Zhang, J. editor. PEM Fuel Cell Electrocatalysts & Catalyst Layers - Fundamentals & Applications. London: Springer; 2008. p. 965-1002.
[19] Zhang, J., Wu, J., Zhang, H., Zhang, J. PEM Fuel Cell Testing & Diagnosis. Elsevier; 2013. p. 2-42.,11
[20] V. Ramani, *Electrochem. Soc. Interface*, **15** (2006) 41-44.
[21] X. Ren, T.E. Springer, T.A. Zawodzinski, S. Gottesfeld, *J. Electrochem. Soc.*, **147** (2000) 466-474.
[22] X. Ren, T.E. Springer, S. Gottesfeld, *J. Electrochem. Soc.*, **147** (2000) 92-98.
[23] K. Scott, W.M. Taama, P. Argyropoulos, K. Sundmacher, *J. Power Sources*, **83** (1999) 204-216.
[24] B. Gurau, R. Viswanathan, R. Liu, T.J. Lafrenz, K.L. Ley, E.S. Smotkin, *J. Phys. Chem. B*, **102** (1998) 9997-10003.
[25] M. Watanabe, M. Uchida, S. Motoo, *J. Electroanal. Chem.*, **229** (1987) 395.
[26] J.B. Kerr Group, *unpublished results*.
[27] K.D. Kreuer, A. Fuchs, M. Ise, M. Spaeth, J. Maier, *Electrochim. Acta*, **43** (1998) 1281-1288.
[28] M.F.H. Schuster, W.H. Meyer, *Annu. Rev. Mater. Res.*, **33** (2003) 233-261.
[29] M.L. Hoarfrost, M.S. Tyagi, R.A. Segalman, J.A. Reimer, *Macromolecules*, **45** (2012) 3112-3120.1
[30] M.F.H. Schuster, W.H. Meyer, G. Wegner, H.G. Herz, M. Ise, K.D. Kreuer, J. Maier, *Solid State Ionics*, **145** (2001) 85-92.
[31] M. Schuster, T. Rager, A. Noda, K.D. Kreuer, J. Maier, *Fuel Cells* (2004), in press. (Invited Paper).
[32] M.F.H. Schuster, W.H. Meyer, M. Schuster, K.D. Kreuer, *Chem. Mater.* **16** (2004) 329.
[33] J.C. Perrson, P. Jannasch, *Chem. Mater.*, **15** (2003) 3044.
[34] H.G. Herz, K.D. Kreuer, J. Maier, G. Scharfenberger, M.F.H. Schuster, W.H. Meyer, *Electrochim. Acta.*, **48** (2003) 2165.
[35] A. Noda, A.B. Susan, K. Kudo, S. Mitsushima, K. Hayamizu, M. Watanabe, *J. Phys. Chem. B*, **107** (2003) 4024-4033.
[36] M. Schuster, T. Rager, A. Noda, K.D. Kreuer, J. Maier, *Fuel Cells*, **5** (2005) 355-365.
[37] NMR data - Matt Dodd Thesis/Unpublished results
[38] S.H. de Almeida, Y. Kawano, *J. Therm. Anal. Calorim.,* **58** (1999) 569.
[39] I.D. Stefanithis, K.A. Mauritz, *Macromolecules*, **23** (1990) 2397.
[40] C.A. Wilkie, J.R. Thomsen, M.L. Mittleman, *J. Appl. Polym. Sci.*, **42** (1991) 901.

[41] S.J. Osborn, M.K. Hassan, G.M. Divoux, D.W. Rhoades, K.A. Mauritz, R.B. Moore, *Macromolecules.*, **40** (2007) 3886.
[42] K.A. Page, K.M. Cable, R.B. Moore, *Macromolecules.*, **38** (2005) 6472.
[43] R.B. Moore, K.M. Cable, T.L. Croley, *J. Membr. Sci.,* **75** (1992) 7-14.
[44] K.A. Page, F.A. Landis, A.K. Phillips, R.B. Moore, *Macromolecules.*, **39** (2006) 3939.
[45] Chartoff, R.P., Menczel, J.D. and Dillman, S.H. (2008) Dynamic Mechanical Analysis (DMA), in Thermal Analysis of Polymers: Fundamentals and Applications (eds J. D. Menczel and R. B. Prime), John Wiley & Sons, Inc., Hoboken, NJ, USA. doi: 10.1002/9780470423837.ch5.
[46] T. Kyu, M. Hashiyama, A. Eisenberg, *Can. J. Chem.,* **61** (1983) 680.
[47] D.J. Burnett, A.R. Garcia, F. Thielmann, *J. Power Sources.*, **160** (2006) 426.
[48] K.S.W. Sing, D.H. Everett, R.A.W. Haul, L. Moscou, R.A. Pierotti, J. Rouquérol, T. Siemieniewska, *Pure & Appl. Chem.,* **57** (1985) 603.
[49] A. Kusoglu, A. Webber, (2012) Water Transport and Sorption in Nafion® Membrane, in Polymers for Energy Storage and Delivery: Polyelectrolytes for Batteries and Fuel Cells. (eds K.A. Page, C.L. Soles, and J. Runt), American Chemical Society, Washington, DC. doi: 10.1021/bk-2012-1096.ch11.
[50] A. Kusoglu, A. Kwong, K.T. Clark, H.P. Gunterman, A.Z. Weber, *J Electrochem. Soc.,* **159** (2012) F530.
[51] K.R. Cooper, *J. Electrochem. Soc.,* **157** (2010) B1731.
[52] B.S. Pivovar, Y.S. Kim, *J. Electrochem. Soc.*, **154** (2007) B739.
[53] J. Zhang, Y. Tang, C. Song, J. Zhang, *J. Power Sourc.,* **172** (2007) 163.
[54] R. Bouchet, S. Miller, M. Douclot. J.L. Souquet, *Solid State Ionics.*, **145** (2001) 69.
[55] P.C. Rieke, N.E. Vanderborgh, *J. Memb. Sci.,* **32** (1987) 313.
[56] A. Kusoglu, S. Savagatrup, K.T. Clark, A.Z. Weber, *Macromolecules,* **45** (2012) 7467.
[57] G. Gebel, P. Aldebert, M. Pineri. *Macromolecules*, **20** (1987) 1425.
[58] L. Rubatat, A.L. Rollet, G. Gebel, O. Diat, *Macromolecules*, **35** (2002) 4050.
[59] M.H. Kim, C.J. Glinka, S.A. Grot, W.G. Grot, *Macromolecules,* **39** (2006) 4775.
[60] H. Baranska, J. Kuduk-Jaworska, S. Cacciari, *J. Raman Spectrosc.*, **28** (1997) 1-7.
[61] C. Yang, P. Costamagna, S. Srinivasan, J. Benziger, A.B. Bocarsly, *J. Power Sources*, **103** (2001) 1-9.
[62] K.R. Cooper, V. Ramani, J.M. Fenton, H.R. Kunz, (2005) Linear Sweep Voltammetry and Cyclic Voltammetry, in Experimental Methods and Data

Analyses for Polymer Electrolyte Fuel Cells., Scribner Associates, Inc., Southern Pines, NC, USA.

[63] R. Makharia, M.F. Mathias, D.R. Baker, *J. Electrochem. Soc.*, **152** (2005) A970-A977.

[64] A. Jackson, K.M. Beers, X.C. Chen, A. Hexemer, J.A. Pople, J.B. Kerr, N.P. Balsara, *Rev. Sci. Instrum.,* **84** (2013) 075114.